Effect of Properties of Metallic Foams on Stiffness and Strength of Sandwich Beams

by

Gaël Gioux

Submitted to the Department of Materials Science and Engineering
in partial fulfillment of the requirements for the Degree of
Master of Science in Materials Science and Engineering

at the

Massachusetts Institute of Technology

February 1999

©1999 Massachusetts Institute of Technology
All rights reserved

Signature of Author .....
Department of Materials Science and Engineering
January 15,1999

Certified by .....
Lorna J. Gibson
Matoula S. Salapatas Professor of Materials Science and Engineering
Thesis Supervisor

Accepted by .....
Linn W. Hobbs
John F. Elliott Professor of Materials
Chairman, Departmental Committee on Graduate Students

Science

EFFECT OF PROPERTIES OF METALLIC FOAMS ON STIFFNESS AND STRENGTH OF SANDWICH BEAMS

by

GAEL GIOUX

Submitted to the Departement of Materials Science and Engineering
on January 15, 1999 in partial fulfillment of the
requirements for the Degree of Master of Science in
Materials Science and Engineering

ABSTRACT

Polymer foam core sandwich beams typically have many cells through the core thickness so that cell size effects are negligible. In some proposed applications of metallic foam core sandwich beams (for instance, aircraft components) this is not the case. Metallic foams have larger cells than polymer foams (2-5 mm rather than 0.2-1 mm) and the thickness of the structural components may be restricted to roughly 5-15 mm. In this study, we examine cell size effects on the structural response of sandwich beams. Metallic foam cores may be subject to substantial normal as well as shear stresses. We begin by considering three possible yield criteria for metallic foams, comparing them to biaxial yield data. The most appropriate yield criterion has been used to determine the loads at which sandwich beams fail in a variety of modes (face yield, core yield and core indentation). The effect of the ratio of cell size to specimen size on core shear strength and core indentation strength is studied next. Finally, the effect of cell size to specimen size on the stiffness and failure of sandwich beams is presented.

Thesis supervisor: Lorna J. Gibson

Title: Matoula S. Salapatas Professor of Materials Science and Engineering

Contents

List of Figures

List of Tables

Acknowledgments

First and foremost, I would like to express my deepest gratitude to Professor Lorna Gibson for giving me the opportunity to join her group, and for her constant support, guidance and encouragement.

I am also grateful to the other members of the "Cellular Materials" group, especially Tim McCormack, Emma Shepherdson, Toby Freyman and Wynn Sanders for their valuable discussions, suggestions and comments. I would like to single out Erik Andrews for his constant help and multiple contributions to this work.

I also wish to thank Mr. John Di Francesco and Mr. John Kane for their assistance in several parts of the technical preparation of my experiments.

Finally, I would like to acknowledge the financial support of ARPA Contract number N00014-96-1-1028.

Chapter 1

Introduction

1.1 Aluminum foams

1.1.1 Description and processes of fabrication

Cellular structures, natural or man-made, represent an important class of materials, from wood to polymeric foams. Among them, metallic foams have appeared recently in the field of man-made materials. Foams can be made out of a number of metals, and several applications have been suggested for aluminum foams, which are the subject of this study.

Several processes are available for the production of aluminum foams (M.F. Ashby et al., 1998) :

- Blowing gas in molten aluminum (alloyed with compounds such as SiC or Al_2O_3 to stabilize the bubbles) and cooling down the material.
- Mixing aluminum powder with a powdered foaming agent (like TiH_2), cold compacting the mixture, then heating it to the temperature where the foaming agent releases hydrogen in the aluminum as it softens. The material expands with the hydrogen bubbles; cooling it, while controlling the pressure, produces the foam.
- A similar process consists of stirring the foaming agent into a mixture of molten aluminum and calcium. Cooling under controlled pressure allows producing the foam.
- A mold is made around a polymeric foam, which is burnt off before infiltrating with molten aluminum. The structure generated with this method can be very regular.

Two main kinds of foam structures can be produced: open- and closed-celled (Fig 1.1 and 1.2). The properties and uses of each are different. Aluminum foams typically have relative densities between 0.02 and 0.35 [1]. Their properties depend on several factors: the properties of the alloy used, the relative density of the foam, and the structure of the foam.

[1]The relative density is defined as the ratio of the density of the foam to that of the solid material the foam is made of (ρ^*/ρ_s)

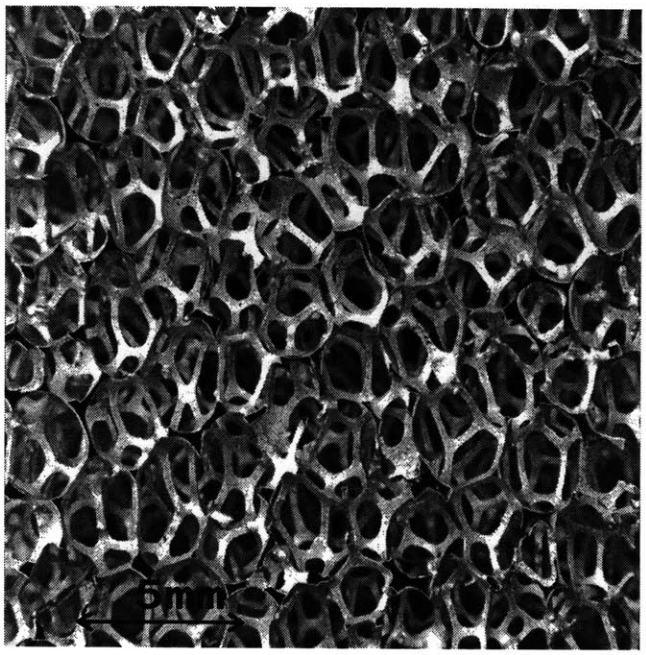

Figure 1.1: Open-cell foam (Duocel) $\rho^\star/\rho_s = 0.08$

1.1.2 Typical mechanical properties

Fig. 1.3 shows a schematic of a stress-strain curve from a typical uniaxial compression test on a metallic foam. After an elastic part (slope $E^\star$), the stress reaches a plateau ($\sigma^\star_{pl}$), at which point the cells collapse plastically. The strain then increases with no or very little increase in the stress, until the foam densifies, at which point the foam begins behaving more like a dense solid.

Several mechanical properties characterize this curve: the Young's modulus $E^\star$, the plateau stress $\sigma^\star_{pl}$ and the densification strain ϵ_D. For an ideal foam, these properties, as well as the shear modulus $G^\star$, the bulk modulus $K^\star$, Poisson's ratio

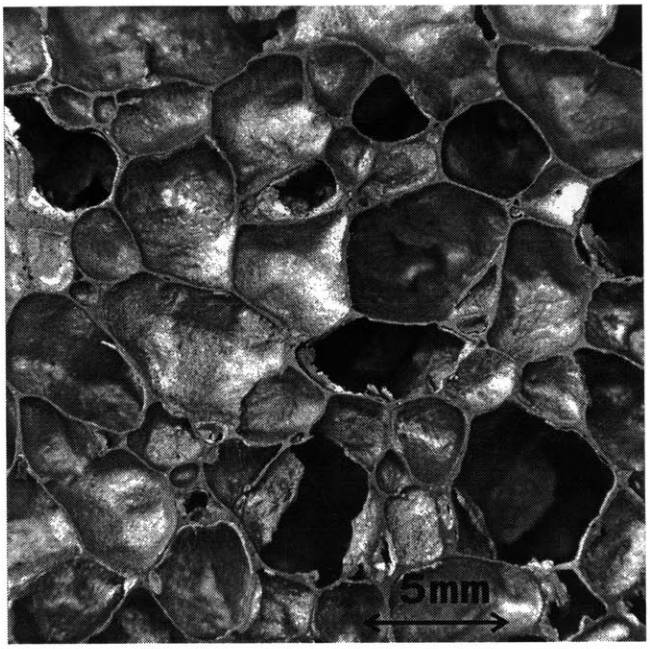

Figure 1.2: Closed-cell foam (Alporas) $\rho^\star/\rho_s = 0.08$

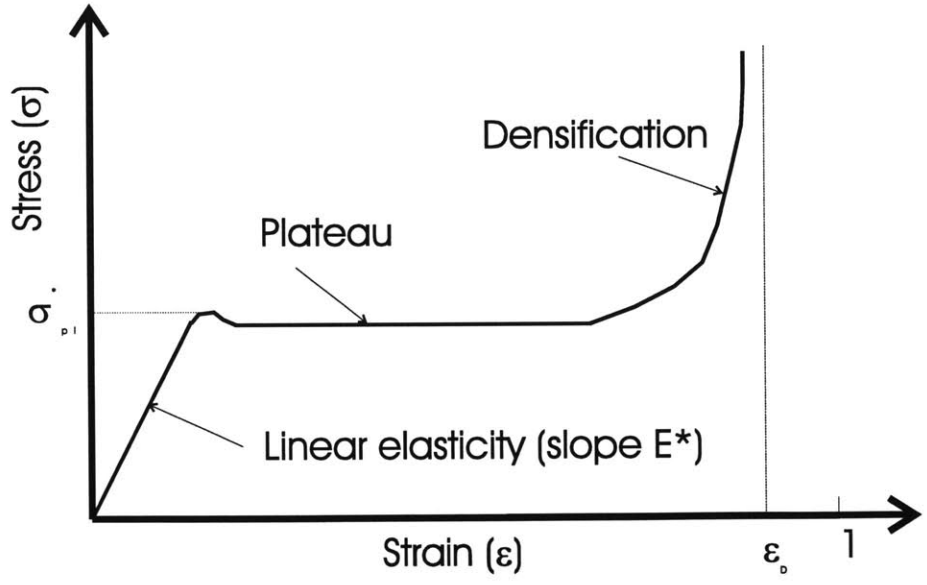

Figure 1.3: Typical stress-strain curve of a metallic foam

$\nu^\star$, can be related to the relative density of the foam (Gibson and Ashby, 1997). For open cell foams:

$$\frac{E^\star}{E_S} \approx \left(\frac{\rho^\star}{\rho_S}\right)^2, \tag{1.1}$$

$$\frac{\sigma^\star_{pl}}{\sigma_{ys}} \approx 0.3\left(\frac{\rho^\star}{\rho_S}\right)^{3/2}, \tag{1.2}$$

$$\epsilon_D = 1 - 1.4\left(\frac{\rho^\star}{\rho_S}\right), \tag{1.3}$$

$$\frac{G^\star}{E_S} \approx \frac{3}{8}\left(\frac{\rho^\star}{\rho_S}\right)^2, \tag{1.4}$$

$$\frac{K^\star}{E_S} \approx \frac{1}{9}\left(\frac{\rho^\star}{\rho_S}\right), \tag{1.5}$$

$$\nu^\star \approx \frac{1}{3}, \tag{1.6}$$

where E_S and σ_{ys} are the Young's modulus and the yield strength of the dense solid the foam is made of.

For a closed-cell foam, the fraction ϕ of the solid that is contained in the cell edges ($1-\phi$ is the fraction of solid in the faces) is introduced:

$$\frac{E^\star}{E_S} \approx \phi^2\left(\frac{\rho^\star}{\rho_S}\right)^2 + (1-\phi)\frac{\rho^\star}{\rho_S}, \tag{1.7}$$

$$\frac{G^\star}{E_S} \approx \frac{3}{8}\left\{\phi^2\left(\frac{\rho^\star}{\rho_S}\right)^2 + (1-\phi)\frac{\rho^\star}{\rho_S}\right\}. \tag{1.8}$$

The other properties are the same as in the case of open-cell foam.

In this thesis, two foams will be studied. The first one, called Alporas, is produced in Japan by Shinko Wire,Ltd. It is a closed-cell foam, with a density varying between 0.2 g/cc and 0.25 g/cc (8% relative density). Its main properties are gathered in Table 1.1. A more complete list of its properties can be found in Appendix A. The other foam studied in this thesis is an open-cell one, produced by ERG, and is named Duocel. It covers a density range between 0.15 and 0.4 g/cc ($\rho^\star/\rho_s =$ 0.055 to 0.15). As for the Alporas foam, this study focused on the 0.2 density (8% relative density). Its main properties are also in Table 1.1, and the more complete list is in Appendix A.

Table 1.1: Main properties of Alporas and Duocel foams

Property	Alporas	Duocel
Material	Al, Al-Ti-Ca(16%), Al-Fe(0.6%)	Al 6061T6
Relative density	$\approx$ 8%	7-8%
Structure	closed cell	open cell
Young's modulus	$\approx$ 1 GPa	$\approx$ 0.5 GPa
Compressive strength	$\approx$ 1.5 MPa	$\approx$ 1 MPa
Densification strain	$\approx$ 65 %	$\approx$ 65 %

1.1.3 Applications

Several uses have been proposed for aluminum foams. The list that follows is not exhaustive and only aims to give an overview of the possible applications.

- **Structural applications:** Aluminum foams have the advantage of being light compared to the dense material, and remain stiff enough for several structural applications. It can be used in the place of honeycomb materials, with the advantage of providing roughly isotropic properties. Typically, aluminum foams can be used in sandwich panels, where they stiffen the structure without adding too much weight.

- **Shock absorption:** The special shape of the stress-strain curve, with a stress plateau lasting over a large range of strain, makes foams very useful for shock absorption applications. Over this plateau, the foam absorbs the energy of the shock, while the stress on the device remains constant. This protection from the foam structure is gained with a small addition of weight, and this could be used in the automobile industry for instance.

- **Other applications:** Depending on the nature of the foam (open or closed cells), other specific applications can be thought of. For example, closed cell foam is currently used as a sound absorption device. The surface of foam plates is crushed to open small cracks, where the sound enters. It is then dissipated in the foam, offering noise protection to the other side of the panel. Open cell foams, with their high thermal conductivity and ability to pass a fluid between the cells, can be used for heat dissipation devices.

1.2 Literature review

1.2.1 Uniaxial behavior

Uniaxial behavior of foams has been modeled by Gibson and Ashby (1997). Equations 1.1, 1.2, 1.3, 1.4, 1.5 and 1.6 have been derived using dimensional analysis of simplified cubic models of foam structures, extending results from the analysis of honeycombs to generalize them in three dimensions. Other equations have also been derived to model the collapse of other kinds of foams (elastomeric foams which collapse elastically or brittle foams). Several results from experimental tests are gathered and most of them fit well with the theory.

The tensile behavior of foams has been studied in the same reference. The elastic part of the stress-strain curve is similar to that in compression. The slope of the elastic part is $E^\star$ defined by equation 1.1, and the equations for the elastic properties $G^\star$, $K^\star$ and $\nu^\star$ are the same in tension as in compression. After the elastic part, the behavior of the foam depends on the type of foam considered. For elastomeric foams, the collapse occurs when:

$$\frac{\sigma^\star_{el}}{E_S} = 0.05 \left(\frac{\rho^\star}{\rho_s}\right)^2. \tag{1.9}$$

For foams failing by plastic collapse (for instance metallic foams), the failure happens

when:

$$\frac{\sigma^\star}{\sigma_{ys}} \approx 0.3 \left(\frac{\rho^\star}{\rho_s}\right)^{3/2}. \tag{1.10}$$

As for brittle foams, the theory of fracture properly describes their failure. For open-cell foams, Gibson and Ashby showed that the fracture toughness $K^\star_{IC}$ was given by:

$$K^\star_{IC} = C\sigma_{fs}\sqrt{\pi l}\left(\frac{\rho^\star}{\rho_s}\right)^{3/2}, \tag{1.11}$$

where C is a constant, σ_{fs} is the modulus of rupture of the material the foam is made of and l is the average length of a cell in the foam.

Tensile fatigue of foams was also analyzed. The theory predicts that the Paris law for foams can be written as:

$$\frac{\mathrm{d}a}{\mathrm{d}N} = l\left(\frac{C}{\Delta\epsilon_f E_S\sqrt{\pi l}}\left(\frac{\rho_s}{\rho^\star}\right)^3\right)^u (\Delta K_I)^u, \tag{1.12}$$

a being the crack length, N the number of cycles, $\Delta\epsilon_f$ the strain which will cause failure in one-half cycle, u and C are constants.

1.2.2 Failure criteria

Several hypothesis and criteria are available to predict the multiaxial failure of foams, based on different approaches. The first one was elaborated by Gibson and Ashby

(1997) for every kind of failure of mechanism which can be found in foam materials, depending on their density and on the foamed base material. Elastic buckling, plastic yielding, brittle crushing or brittle fracture are the different failure modes modeled. This hypothesis is based on the analysis of regular honeycombs (2 dimensions); these results are then generalized for perfect, isotropic and homogeneous foam materials, using dimensional arguments.

Regular honeycombs under biaxial loading fail when the combined bending and axial stresses in the cell walls reach the yield stress of the solid. The moment in the walls is proportional to the deviatoric stress σ_d (varying as $\sigma_1 - \alpha\sigma_2$, $\alpha > 0$). The axial stress in the walls is proportional to the mean stress σ_m (varying as $\sigma_1 + \beta\sigma_2$, $\beta > 0$). When a function of these two stresses reaches a critical value, the honeycomb fails. The yield function can be calculated exactly with all the coefficients for honeycombs. It is shown in particular that this function has a dependence on the relative density of the honeycomb.

The same type of analysis was used with foams. A similar equation was assumed for foams, depending on σ_d and on σ_m^2, with the same dependence on the relative density $\rho^\star/\rho_s$. The unidentified coefficients are determined using limit cases. The following equation was found to describe the plastic yield surface for foams:

$$\pm\frac{\sigma_e}{\sigma^\star_{pl}} + 0.81\left(\frac{\rho^\star}{\rho_s}\right)\left(\frac{\sigma_m}{\sigma^\star_{pl}}\right)^2 = 1 \tag{1.13}$$

The same process was used for the different modes of failure, and the following equations were found, for brittle crushing:

$$\pm\frac{\sigma_e}{\sigma^\star_{cr}} + 0.6\left(\frac{\rho^\star}{\rho_s}\right)^{1/2}\left(\frac{\sigma_m}{\sigma^\star_{cr}}\right) = 1, \tag{1.14}$$

and for brittle fracture:

$$\sigma_1 = \sigma^\star_{fr} = \frac{K^\star_{Ic}}{\sqrt{\pi a}} = \frac{0.65\sigma_{fs}\sqrt{\pi l}\left(\frac{\rho^\star}{\rho_s}\right)^{3/2}}{\sqrt{\pi a}}. \tag{1.15}$$

In these equations σ_e is the von Mises equivalent stress, σ_m the mean stress, $\sigma^\star_{pl}, \sigma^\star_{cr}$ and $\sigma^\star_{fr}$ are the uniaxial plastic collapse, brittle crushing and tensile fracture strengths of the foam, $K^\star_{Ic}$ is the fracture toughness of the foam, $\rho^\star/\rho_s$ is the relative density of the foam, l is the cell size and a is the half crack length. As for elastic buckling, it appears approximately when one of the principal stresses reaches a limit, the value of which is almost independent of the other principal stress (hydrostatic buckling strength = 0.88 * uniaxial buckling strength). Triantafillou (1989) has modified these equations to take into account the anisotropy of the real foams (see properties in Appendix A). In equation 1.13, $\sigma_e/\sigma^\star_{pl}$ was replaced by:

$$\tilde{\sigma_e} = \sqrt{\frac{1}{2}\left[\left(\frac{\sigma_1}{\sigma^\star_{pl1}} - \frac{\sigma_2}{\sigma^\star_{pl2}}\right)^2 + \left(\frac{\sigma_2}{\sigma^\star_{pl2}} - \frac{\sigma_3}{\sigma^\star_{pl3}}\right)^2 + \left(\frac{\sigma_3}{\sigma^\star_{pl3}} - \frac{\sigma_1}{\sigma^\star_{pl1}}\right)^2\right]}, \tag{1.16}$$

and $\sigma_m/\sigma^\star_{pl}$ by:

$$\tilde{\sigma_m} = \frac{1}{3}\left(\frac{\sigma_1}{\sigma^\star_{pl1}} + \frac{\sigma_2}{\sigma^\star_{pl2}} + \frac{\sigma_3}{\sigma^\star_{pl3}}\right). \tag{1.17}$$

The same substitution could be made in equation 1.14, using $\sigma^\star_{cr}$ instead of $\sigma^\star_{pl}$. For aluminum foams studied here, failure occurs mainly due to plastic yielding, so the anisotropic version of the useful failure equation is:

$$\pm\tilde{\sigma_e} + 0.81\left(\frac{\rho^\star}{\rho_s}\right)\tilde{\sigma_m}^2 = 1 \tag{1.18}$$

A second approach, based on phenomenological considerations, has also been used to characterize failure of metallic foams. These criteria can all be written at failure as:

$$f(\bar{\sigma}, \kappa) = 0,$$

where $\bar{\sigma}$ represents the stress tensor, and κ a set of variables the number and nature of which depend on the criterion. An example of one such criterion is that developed by Drucker and Prager (1952) for porous materials such as soils. To account for

the particularity of porous materials, where mean stress, as well as the equivalent stress, plays a role in yielding, the Drucker-Prager criterion was written as follows:

$$f = \sigma_e + \gamma\sigma_m - d, \tag{1.19}$$

where γ and d are constants. A similar approach has been used to describe the compaction of porous powders, with both von Mises equivalent stress and mean stress involved, but with different powers than in equation 1.19 (Fleck et al. 1992) .

$$f = \left(\frac{\sqrt{5}\sigma_m}{3p_Y}\right)^2 + \left(\frac{5\sigma_e}{18p_Y} + \frac{2}{3}\right)^2 - 1, \tag{1.20}$$

where p_Y is the yield strength under hydrostatic pressure.

Inspired by these criteria combining von Mises equivalent stress and mean stress, two new criteria have been developed recently to describe behavior of metallic foams. The first one is a modified version of the Drucker-Prager criterion, which allows different values for the uniaxial compressive and tensile strengths. Miller's criterion (Miller and Hutchinson, 1998) was formulated as follows:

$$f = \sigma_e + \gamma\sigma_m + \frac{\alpha}{d}\sigma_m^2 - d. \tag{1.21}$$

In this equation, the constants γ, α and d are functions of the ratio of the uniaxial

compressive to tensile strengths ($\beta = \frac{\sigma_c}{\sigma_t}$), and of the plastic Poisson's ratio ν^p. Whereas Drucker-Prager criterion, by the choice of γ, fixes a value for ν^p, Miller's criterion introduces a new variable, such that γ is now calculated from both β and ν^p. The values of the constants γ, α and d are given by:

$$\begin{aligned}
\gamma &= \frac{6\beta^2 - 12\beta + 6 + 9(\beta^2 - 1)/(1+\nu^p)}{2(\beta+1)^2}, \\
\alpha &= \frac{45 + 24\gamma - 4\gamma^2 + 4\nu^p(2+\nu^p)(-9+6\gamma+\gamma^2)}{16(1+\nu^p)^2}, \\
d &= d_0\sigma_c, \\
\text{with } d_0 &= \frac{1}{2}\left(1 - \gamma/3 + \sqrt{(1-\gamma/3)^2 + 4\alpha/9}\right).
\end{aligned}$$

Dividing equation 1.21 by σ_c, and replacing σ_e/σ_c and σ_m/σ_c by expressions similar to equations 1.16 and 1.17, with σ_{ci} instead of σ_{pli} the following failure criterion is obtained:

$$\tilde{\sigma_e} + \gamma\tilde{\sigma_m} + \frac{\alpha}{d_0}\tilde{\sigma_m}^2 = d_0 \tag{1.22}$$

The second new criterion has been proposed by Deshpande and Fleck (1998) and is based on the powder compaction model. It can be written as follows:

$$f = \hat{\sigma} - Y \tag{1.23}$$

where Y is the uniaxial yield strength (same as $\sigma_{pl}^{\star}$) and:

$$\hat{\sigma}^2 = \frac{1}{1+(\alpha/3)^2}\left[\sigma_e^2 + \alpha^2\sigma_m^2\right]$$

where α depends on the foam's plastic Poisson's ratio ν^p by the following relation:

$$\alpha = 3\left(\frac{1/2-\nu^p}{1+\nu^p}\right)^{1/2}$$

It is possible to divide equation 1.23 by Y, square the obtained equation and introduce $\tilde{\sigma_e}$ and $\tilde{\sigma_m}$ defined by equations 1.16 and 1.17 in the criterion. A version of Deshpande and Fleck criterion, taking anisotropy into account can be written as follows:

$$\frac{1}{1+(\alpha/3)^2}\left[\tilde{\sigma_e}^2 + \alpha^2\tilde{\sigma_m}^2\right] = 1 \tag{1.24}$$

Note that Miller's criterion allows different tensile and compressive strengths, while Deshpande and Fleck's does not.

Previous studies (Shaw and Sata, 1996, Patel , 1969, Fortes et al., 1989, Triantafillou and al., 1989, Triantafillou and Gibson, 1990) have shown a good agreement between equation 1.13, 1.14 and 1.15 and the data collected with different kinds of foams (flexible polyethylene, rigid polyurethane, polystyrene, aluminum and reticulated vitreous carbon) under biaxial loads and axisymmetric triaxial loads, except

in hydrostatic tension.

1.2.3 Sandwich beams

The behavior and failure of sandwich beams with foam core have already been studied in the literature. The results often depend on the type of experiment considered (3-point bend test, 4-point bend tests, cantilever beam,...). Three-point bending on sandwich beams has been studied more specifically in the literature. Therefore, this section is dedicated to the description of what has been observed in three-point bending experiments on sandwich beams with a foam core.

- **Elastic behavior:**

  The compliance of a sandwich beam has been derived by Allen (1969), using the equivalent flexural rigidity $(EI)_{eq}$ and the equivalent shear rigidity $(AG)_{eq}$ defined by:

$$(EI)_{eq} = \frac{E_f b t^3}{6} + \frac{E_c b c}{12} + \frac{E_f b t d^2}{2}, \tag{1.25}$$

$$(AG)_{eq} = \frac{b d^2 G_c^\star}{c}, \tag{1.26}$$

  where b is the width of the specimen, t the thickness of the face, c the thickness of the core (Fig 1.4), $d = c + t$, E_f and E_c are the Young's modulus of the faces

and of the core respectively, and $G_c^\star$ is the shear modulus of the core.

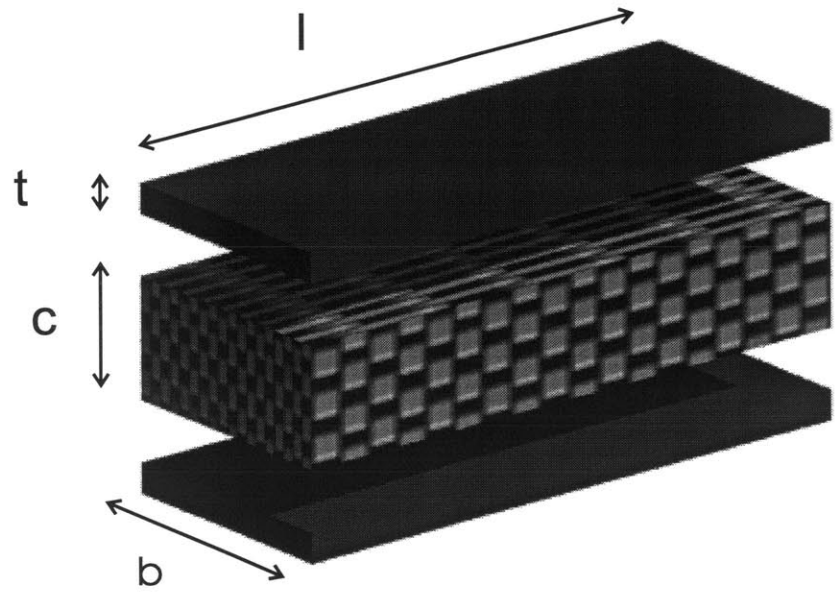

Figure 1.4: Dimensions of the sandwich beam

For typical sandwich structures, the faces are thin compared the core ($c >> t$), and the faces are much stiffer than the core ($E_f >> E_c$), allowing the following simplifications to be made:

$$(EI)_{eq} = \frac{E_f b t c^2}{2} \tag{1.27}$$

$$(AG)_{eq} = bcG_c^\star \tag{1.28}$$

As described by Allen , the deflection δ provoked by the applied force P in a three-point bend test, with the load applied along a line, can be decomposed

into two parts, one due to bending and one due to shearing:

$$\delta = \delta_b + \delta_s = \frac{Pl^3}{48(EI)_{eq}} + \frac{Pl}{4(AG)_{eq}}.$$

Therefore, the compliance can be written:

$$\frac{\delta}{P} = \frac{2l^3}{48E_f btc^2} + \frac{l}{4bcG_c^\star}. \tag{1.29}$$

- **Failure:**

  Sandwich beams can fail by several modes. Studies of sandwich failure resulted in what is called "failure maps", which are graphs mapping the different modes of failure depending on the parameters of the sandwich: type of test (3-point bend test, 4-point bend test,...), thickness of the core, thickness of the plates, length of the beam, shape of the support, and other parameters. To produce such a map, the failure loads for every mode have to be known as a function of all the sandwich parameters. For a given set of parameters, there is a mode with a lower failure load than the other modes. Picking for every set of parameters the associated mode defines the different areas of the map.

  The stresses in the core and in the faces have been derived by Allen (1969). The maximum normal stresses in the faces (σ_f) and in the core (σ_c) are related

to the applied moment M by:

$$\begin{aligned} \sigma_f &= \frac{MyE_f}{(EI)_{eq}} = \frac{M}{btc}, \\ \sigma_c &= \frac{MyE_c^\star}{(EI)_{eq}} = \frac{M}{btc}\frac{E_c^\star}{E_f}, \end{aligned}$$

assuming that equation 1.27 is valid (y is the distance from the neutral axis, and the maximum face normal stress is reached at $y = c+t$ while the maximum core normal stress is reached at $y = c$). The shear stress varies parabolically through the face and the core:

$$\tau = \frac{V}{D}\left[E_f\frac{td}{2} + \frac{E_c}{2}\left(\frac{c^2}{4} - y^2\right)\right]$$

where V is the shear force and D is given by:

$$D = \frac{E_f bt^3}{6} + \frac{E_f btd^2}{2} + \frac{E_c bc^3}{12}$$

But considering that typically the faces are much stiffer and thinner than the core, it can be assumed that the shear stress is linear in the faces and constant in the core:

$$\tau_c = \frac{Q}{bc},$$

where Q is the maximum shear force in the beam.

As described by Gibson and Ashby (1997), the failure of sandwich in three-point bend tests can happen with several modes: face yielding, face wrinkling, core shear, core fracture or bond failure. They derived the different failure loads for each mode of failure for several loading conditions. For the three-point bend tests, the results were the following ones:

- Face yielding: $P = 4bc(t/l)\sigma_{yf}$;
- Face wrinkling: $P = 2.28bc(t/l)E_f^{1/3}E_s^{2/3}(\rho_c^\star/\rho_s)^{4/3}$;
- Core shear: $P = C_{11}2bc\sigma_{ys}(\rho_c^\star/\rho_s)^{3/2}$;
- Core fracture: $P = C_8 2bc\sigma_{fs}(\rho_c^\star/\rho_s)^{3/2}\sqrt{l^\star/a}$;
- Bond failure: $P = 4bc(t/l)\sqrt{(G_c E_f)/t}$.

In those equations, b is the width of the sandwich, c the thickness of the core, t the thickness of each plate, E_f and E_s respectively the Young's moduli of the plates and of the solid the foam is made of, $\rho_c^\star/\rho_s$ is the relative density of the foam, σ_{yf} is the yield strength of the plates, σ_{ys} that of the solid the foam is made of, σ_{fs} is the modulus of rupture of the foam base material, G_c is the toughness of the adhesive, and C_{11} and C_8 are constants of proportionality. Several experiments realized on different geometries of sandwich beams with aluminum faces and rigid polyurethane foam cores showed that three main

modes can be expected from 3-point bend tests: face yield, face wrinkling and core shear failure.

Here, we are interested in aluminum face / aluminum foam core sandwich panels. The critical failure modes in this case are face yield, indentation and core shear. The failure loads for each of these modes have been derived by Miller (1998b). For typical aluminum foam core properties, the second term of equation 1.25 is significant, so that it must be included in the stress calculations. In addition, the normal stresses in the core are comparable to the shear stresses. Face yield failure is straightforward: it is found simply by equalizing the normal stress in the face with the yield strength of the face. Indentation and core shear failure are more complicated, as they involve multiaxial stress states. Miller has used a finite element parametric study for indentation case, using the multiaxial criterion (equation 1.21) derived by Miller and Hutchinson and described in section 1.2.2. Core shear failure is also modelled using finite elements, using the multiaxial yield criterion (Eqn 1.21). The geometry of those simulations is shown in Fig. 1.5: loads are applied via parallelepipedic pads bonded to the plates.

Defining:

$$\tilde{P} = \frac{P}{bl\sigma_c},$$

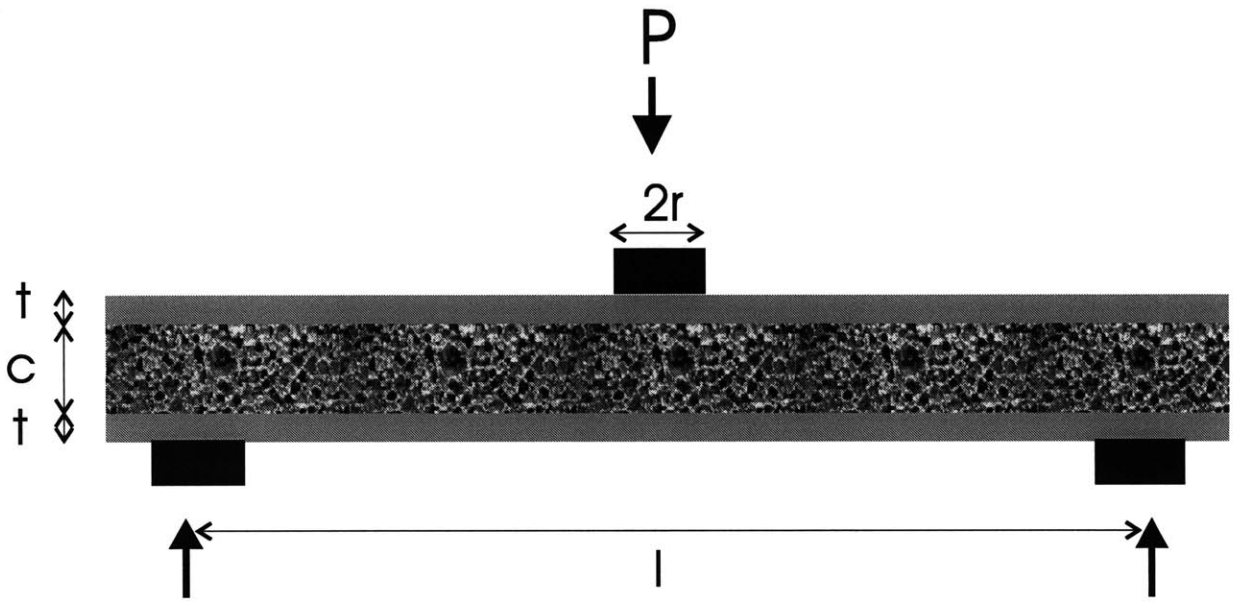

Figure 1.5: Sandwich geometry used by Miller for failure maps

where P is the applied load, b is the width of the specimen, l is its length, and σ_c is the compressive strength of the foam, Miller found the following values for the failure loads:

- Bending (face yield) failure mode:

$$\tilde{P}_b = 4\frac{tc}{l^2}\frac{\sigma_y}{\sigma_c}, \tag{1.30}$$

- Indentation:

$$\tilde{P}_i = 1.4\left(\frac{1}{\sqrt{2}}\sqrt{\frac{\sigma_y}{\sigma_c}}\frac{t}{l} + \frac{r}{l}\right) \tag{1.31}$$

– Shear failure of the core:

$$\tilde{P}_s = \frac{d_0}{2}\left(\frac{-b+\sqrt{b^2+4a}}{a}\right) \tag{1.32}$$

σ_y is the yield strength of the faces, d_0 is defined in equation 1.21. a and b are defined as follows:

$$\begin{aligned} a &= \frac{\alpha}{9}(1+\nu^p)^2 A^2, \\ b &= \frac{\gamma}{3}(1+\nu^p)A + \sqrt{3B^2 + A^2(\nu^{p2} - \nu^p + 1)}. \end{aligned}$$

α and γ are defined in equation 1.21. ν^p is the plastic Poisson's ratio and A and B are defined by:

$$\begin{aligned} A &= \frac{l^2 E_c}{4tcE_f} \\ B &= \frac{l}{2c} \end{aligned}$$

Experiments from McCormack (1999) on Alporas foam have validated the failure maps obtained from the failure loads above. Fig 1.6 shows an example of a typical failure map obtained from the equations above.

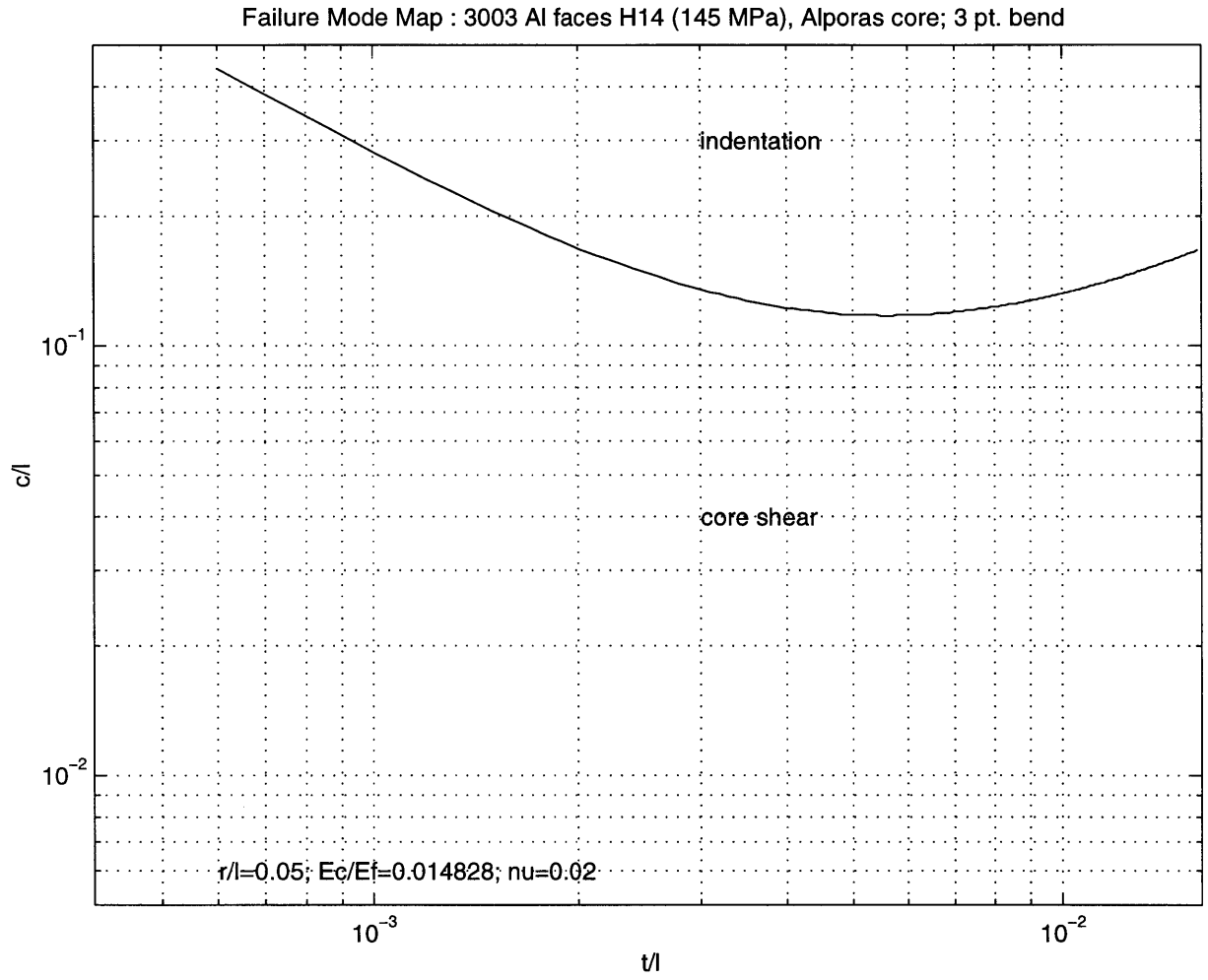

Figure 1.6: Failure map obtained from Miller's equations for failure

1.2.4 Size effects

Size effects in cellular materials have inspired several articles in the last few years. At least two factors contributing to create these size effects have been described, analyzed and modelled in the literature.

When an element (beam, rod,...) is cut from a piece of foam, there is a layer on the surface where the cells are poorly connected, where the cells may have been damaged by the cutting technique used. The mechanical properties of this layer are lower than the ones of the core of the element. Brezny and Green (1990) have analyzed and modelled this phenomenon for beam bending in a brittle foam. In their model, a square cross section beam is described as formed by a core (Young's modulus E_1) surrounded by a layer of damaged cells ($E_2 < E_1$) of constant thickness X. Defining $n = E_2/E_1$, they found that the moment of inertia of the beam is given by:

$$I = \frac{(1-2nX)(1-2X)^3 + 2nX^3}{12} + nX(1-X)^2,$$

making the beam easier to bend, with $n < 1$. The strength of the beam is affected the same way by this size effect. More generally, due to this outer layer of constant thickness, the mechanical properties decrease as the specimen size decreases. Their model gives a good agreement with experimental results obtained with reticulated vitreous carbon beams in three-point bending. This effect was also observed on

closed-cell polymethacrylimide and open-cell copper foams (Anderson et al. 1994).

Another part of the article by Brezny and Green describes the size effect due to the statistical nature of flaws in ceramics. When considering two specimens (same geometry) with different volumes V_1 and V_2 (let's assume $V_1 > V_2$), the probability of finding a larger flaw in specimen 1 is higher than in specimen 2, due to the larger volume considered. The strength of the material increases when the size of the specimen decreases. Brezny and Green assume a Weibull distribution with a modulus m of 15 (typical for the materials they used). The strengths of the two specimens are related by:

$$\frac{\sigma_1}{\sigma_2} = \left(\frac{V_2}{V_1}\right)^{1/m}, \tag{1.33}$$

which means that, for $V_2/V_1 = 10$, there would be a 16% increase in strength from specimen 2 to specimen 1. This effect only appears in brittle specimens, like cellular materials made of ceramics. The conclusion of Brezny and Green work was that bending tests on reticulated vitreous carbon require samples with 15 to 20 cells along its edges.

A size effect in cellular solids is also predicted by Cosserat elasticity, which introduces the local rotation of points in elasticity (Anderson and Lakes 1994):

$$\sigma_{kl} = \lambda\epsilon_{rr}\delta_{kl} + (2\mu + \kappa)\epsilon_{kl} + \kappa\epsilon_{klm}(r_m - \phi_m)$$

$$m_{kl} = \alpha\phi_{r,r}\delta_{kl} + \beta\phi_{k,l} + \gamma\phi_{l,k}$$

where σ_{kl} is the force stress (asymmetric in this theory), m_{kl} is the couple stress, $\epsilon_{kl} = (u_{k,l} + u_{l,k})/2$ is the strain, u being the displacement, ϵ_{klm} is the permutation symbol, ϕ_k is the microrotation, which is distinct from the macrorotation $r_k = \epsilon_{klm}u_{m,l}/2$. $\alpha, \beta, \gamma, \kappa, \lambda$ and μ are the elastic constants. This theory suggests that the elastic moduli increase when the size of specimens decreases (an effect opposite to that predicted by the damaged layer theory). Results from experiments on polymethacrylimide foam show that with specimens prepared with no particular care to avoid surface damage, damaged layer effect is predominant and causes a reduction in modulus as the cell size decreases. However, with specimens prepared with great care, stiffening effects predicted by Cosserat elasticity theory can be observed at small sizes. According to Anderson and Lakes, the size effect due to Cosserat elasticity disappears when more than 3 or 4 cells are considered.

Another theory introducing size effects is the non-local elasticity theory (Andersen and Lakes 1994), where the stress in one point depends of the strain state around the point.

$$\sigma_{ij}(x) = \int_V \{\lambda(|x' - x|)\epsilon_{rr}(x')\delta_{ij} + 2\mu(|x' - x|)\epsilon_{ij}(x')\}\, dV(x')$$

This theory can model different size effect in bending and torsion, with increasing or decreasing moduli as specimen size decreases. However, both this theory and Cosserat theory of elasticity only introduce size effect in elastic properties of materials, not in their strength.

Andrews et al (1998) have shown experimental evidence of the size effects on uniaxial elastic modulus and uniaxial plastic collapse strength of aluminum foams. According to these results, approximately 8 cells are necessary along the edges of the tested specimen to get a behavior similar to that of the bulk. Below that number of cells, the properties of the specimens are poorer.

These results were analyzed using Brezny and Green's method on a foam with a cell size d and a width L. The cell walls in the damaged boundary layer have a reduced stiffness mF/δ $(0 < m < 1)$, F/δ being the stiffness of the individual cell walls. The depth of the boundary layer is proportional to the cell size: depth $= nd$. It was found that:

$$\frac{E}{E_{bulk}} = m + (1-m)\left(1 - \frac{2nd}{L}\right)^2. \tag{1.34}$$

For $m = 0.75$, the number of cells necessary to reach a modulus independent of the size is around 8-10, slightly above the number found experimentally.

In the same work, this size effect on Young's modulus of foam is also compared with the analysis of a two dimensional, hexagonal honeycomb (infinite length, width

W and cell size D), under uniaxial compressive load. When the ratio W/D decreases, it is found that the Young's modulus decreases (at $W/D = 3$, the Young's modulus reaches 82 % of the bulk value).

The same paper mentions an increase of the shear modulus when decreasing the size of the specimens used in a shear test (in the case where the specimens are bonded to plates and relative displacements of the plates put the foam in shear). Brezny and Green's method was also used in this part to characterize this size effect. Considering a foam specimen with a thickness t, bonded to two plates and subject to a shear test, the stiffness of the individual cell walls being F/δ and mF/δ ($m > 1$ to model the "higher" mechanical properties of the outer layer of cells due to their clamping to the plates) on the fixed boundaries (of depth nd, d being the cell size), the following expression was found for the shear modulus:

$$\frac{G}{G_{bulk}} = \frac{1}{1 - 2n\left(1 - \frac{1}{m}\right)\frac{d}{t}}. \tag{1.35}$$

For the size effect on shear modulus, using the same values for m and n as for the Young's modulus, 3 or 4 cells are necessary across the specimens to get the asymptotic value of the modulus.

The same effect was found analyzing a honeycomb similar to the one used in the analysis of the Young's modulus size effect, but this time, placed under shear

loading. The edges of the honeycomb are rigidly attached to the plates transmitting the shear load. When the ratio H/D (H being the thickness of the specimen, D the cell size of the honeycomb) decreases, the shear modulus is found to increase ($H/D = 1$ gives a shear modulus 4.2 times higher than the bulk shear modulus, $H/D = 3$ gives a modulus 1.28 times higher than the bulk one).

Table 1.2 summarizes the different theories presented above on size effects with remarks on each of them.

Table 1.2: The different size effect theories

	Edge effect	Statistical repartition of flaws	Cosserat elasticity	Shear modulus (bonded boundaries)
Number of cells necessary to get bulk properties	15-20 (Brezny and Green) 8-10 (Andrews)		3-4	3-4
Remarks	Predominant effect most of the time	Brittle specimens. High ratio V_1/V_2 needed to observe	Difficult to observe (hidden by other effects) Only predicts effects on elastic moduli	Special case of edge effect

1.3 Objective and Outline

As described in the previous section, the size of a foam piece can have an influence on its mechanical properties. In sandwich structures made with metallic foam cores, the thickness of the foam layer may be in the range of a few cell diameters. The objective of this thesis is to characterize the consequences of the size effects expected from foam structure on the behavior of sandwich beams with foam cores. More precisely, the influence of core thickness on the stiffness and the strength of the beam are studied in this thesis.

Several steps were necessary to achieve that study. As shown in the literature review, several failure criteria are available for the foams. The first step was to determine which failure criterion was to be used for the aluminum foams (Duocel and Alporas). This is the subject of chapter 2. The third chapter is dedicated to the study of the different size effects important in the case of sandwich structures: for the strength of the beam, the influence of the thickness of the core on shear strength is examined. As failure of the beams can also happen by indentation of the core, the influence of the size of the indenter on the indentation strength is also studied in this chapter. All the results from chapter 2 and 3 are used in the following chapter to characterize the influence of the thickness of the core of sandwich beams on its stiffness and strength.

Chapter 2

Failure criterion for metallic foams

2.1 Objective

Foams, and especially the metallic ones, are more and more often used in structural applications which may involve multiaxial loading that could lead to failure of the structure. A multiaxial failure criterion is then necessary to implement in finite elements codes to design structures, including sandwich beams. Here, we assume that the specimens are sufficiently large that the size effect studied in next chapter can be neglected. Several criteria have been proposed and our objective is to compare these criteria, using two different aluminum foams. These foams were submitted to biaxial loads to compare the multiaxial criteria and determine which one describes the data best.

2.2 Materials

Biaxial tests were performed on Alporas and on Duocel foams (relative density: 8 %, cell size: 4.5mm for Alporas, 1.5mm for Duocel) to select one of the available failure criteria. Several geometries were necessary to perform the tests in different stress conditions. Compression-compression tests were performed on cubic specimens, compression-tension tests on dogbone specimens.

The Alporas cubic specimens were prepared by cutting blocks from an Alporas plate, then machining to the final dimensions using a milling machine. The Duocel cubic specimens were prepared by ERG. The average length of the cubes was 45.48 mm (std dev : 0.39) for the Alporas specimens, and 44.41 mm (std dev: 0.03) for the Duocel specimens. The average density for Alporas cubes was 0.216 g/cc (standard deviation: 0.009), while it was 0.217 g/cc (std dev: 0.006) for Duocel cubes. The Alporas dog-bone specimens were prepared using a band saw, and the Duocel bog-bones were prepared by ERG. Their average density was respectively 0.261 g/cc (sdt dev: 0.011) and 0.200 g/cc (std dev: 0.008). According to the results from Andrews et al (1998), the surface preparation of the specimen has little influence on the mechanical properties of the foam materials. The dimensions of the specimens (both the cubes and the dog bones specimens) were chosen so that the size effects studied in the work just mentioned do not appear; that is there was a sufficient

number of cells across the length of the cubes and in the section of the dog-bones specimens (number of cells equal or more than 8 cells).

2.3 Method

Two types of biaxial loads were applied to both Alporas and ERG foams:

- First, cubic specimens were submitted to compressive loads along two directions, using a jig (Fig. 2.1): 2 sets of aluminum plates were used to apply the load on the specimens, and these plates could interpenetrate to allow compressive deformation (15 % strain allowed), thanks to the fingers on each side of the plates.
- Tension-compression tests have been tried on cubic specimens but several problems appeared, mainly due to the bonding of the specimens. These problems were solved using a new geometry more adapted to the goal : dogbone shaped specimens (Fig. 2.2). Compressive loads were applied along one direction using the hydraulic jack with bigger plates than with cubes (102mm long) to cover the whole gage length of the specimens, while tension loads were applied in the other direction, using an Instron testing machine.

Uniaxial compression tests have been done in the two directions with both cubic and dogbone specimens to check that the results were consistent. Vertical loads were

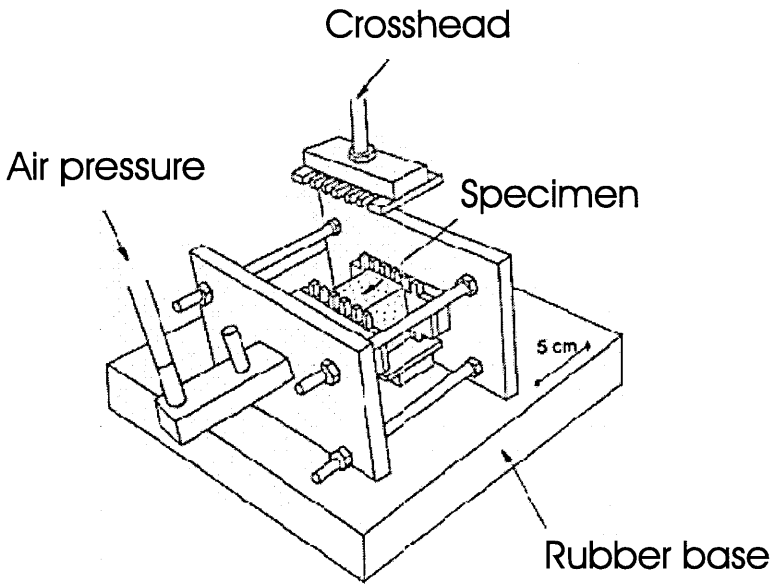

Figure 2.1: Setup for compression-compression tests

applied using an Instron testing machine (model 1361 (cubes), model 1321 (dogbone specimens), Canton, MA) in displacement control with strain rates around $4.10 * 10^{-3}$. Horizontal loads were applied using a hydraulic jack (load control). Loads were read by the means of a 2000 lbs. load cell and a pressure transducer on the hydraulic line. Displacements were obtained from LVDTs (Model 0244, Transtek, Ellington, CT). All the data (loads, displacements) were read through Labview data acquisition system (National Instruments, Austin, TX). From the area of contact between the plates (taking into account the fingers) and the specimens, it was possible to compute the stress in the foam. As ERG is an anisotropic structure, the orientation of the

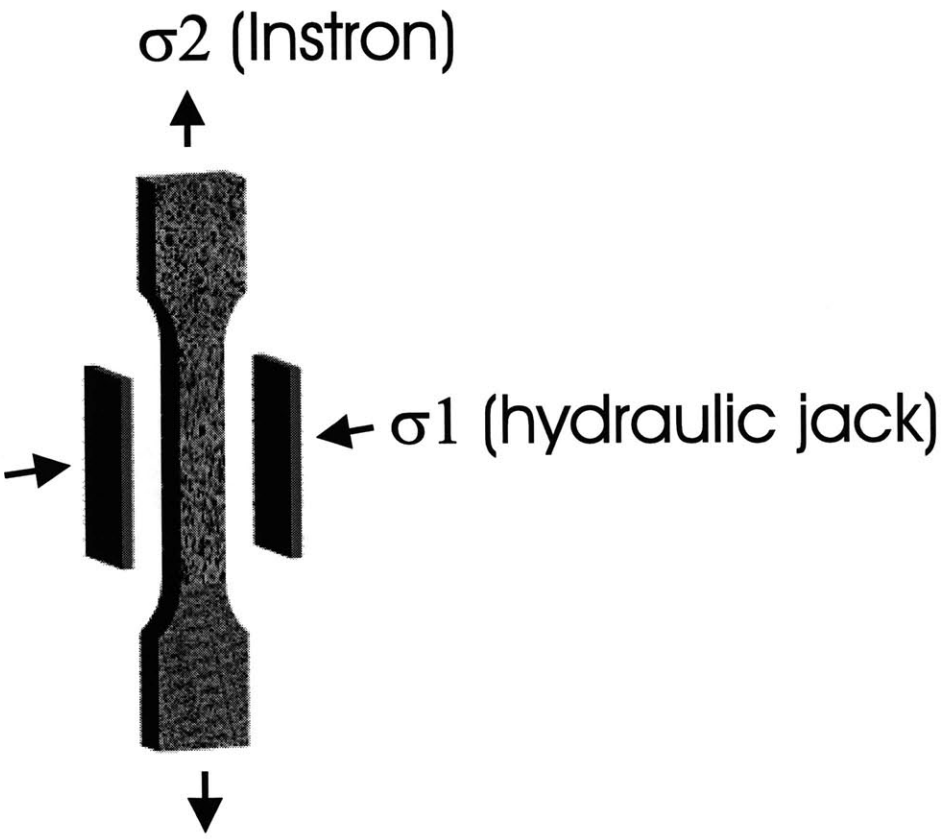

Figure 2.2: Setup for compression-tension tests

specimens was known, and the tests were performed with the vertical direction being the same as the one of the elongation of the cells (σ_2). As for Alporas foam, the anisotropy is not obvious visually, so the cubes were randomly oriented. For Alporas cubes, two series of tests have been performed. The first one was done with the plates of the jig simply resting on the cubes, with frictional constraints. Then, the same experiments were done using grease between the plates and the cubes to lower the influence of friction. With ERG cubes, only the experiments without grease have been done. As for the tension-compression experiments, a layer of grease between the plates and the specimens was used for both Alporas and Duocel. During the test, failure was reached first by applying some load (less than the peak load) along one direction, then keeping the displacement/load constant along that direction, increasing the load/displacement along the other direction until failure occurred. To reach some points of the failure curve, it was sometimes necessary to repeat the direction change several times (for example to reach the shear state, the loads were applied successively along each axis, keeping the displacement/load constant on the other direction). In (σ_1, σ_2) stress space, the experiments would follow successively horizontal and vertical lines.

2.4 Results

Fig 2.3 and 2.4 show typical stress-strain curves obtained in the experiment described above (Fig 2.3: compression-compression, Fig 2.4: tension-compression). At small strains, the material is elastic, then some plasticity occurs before the stress reaches a peak value $\sigma^\star$. For specimens failing in compression, the curve reaches a plateau region, where the stress remains roughly constant as the strain increases. For specimens failing in tension, the material begins to break when the stress reaches the peak value, and the stress decreases when the strain increases further. The failure stress was taken at the peak stress when it existed, or at the intersection of the lines fitted to the stress plateau and to the elastic part of the loading.

In a biaxial test, two stress-strain curves are obtained, which allow the value of the stress in each direction to be obtained when the failure occurs along one of the axes. Fig 2.5 and 2.6 show the different combinations of stress obtained at failure respectively for Alporas and for ERG foams. As the use of grease with the Alporas showed an increase of 25 % in the strength of the foam, comparing to the results with the cubes with no grease, the same ratio has been used with the ERG cubes, which were tested without grease, to take the friction into account and plot only the strength in a "pure" biaxial loading (both original and "corrected" results are plotted). In the Alporas plot, as the direction were not known, the symmetry of two

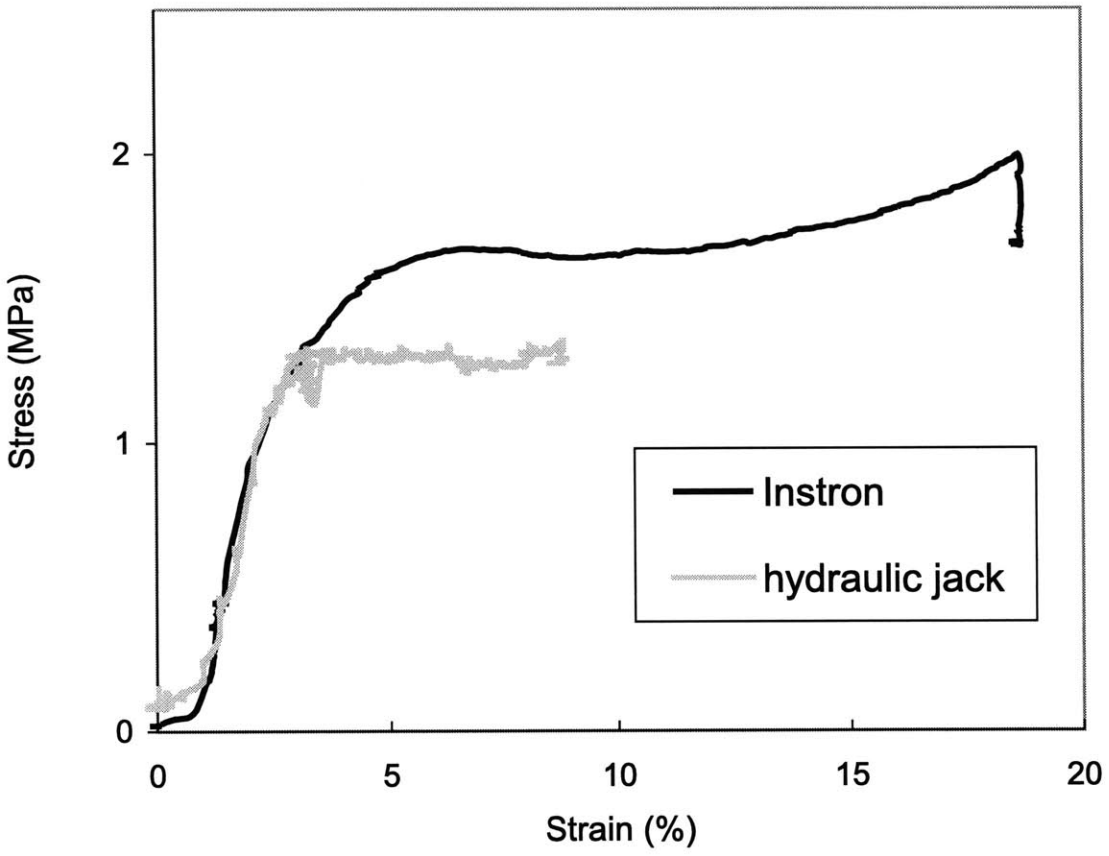

Figure 2.3: Typical biaxial stress-strain curves (compression-compression) for Alporas foam

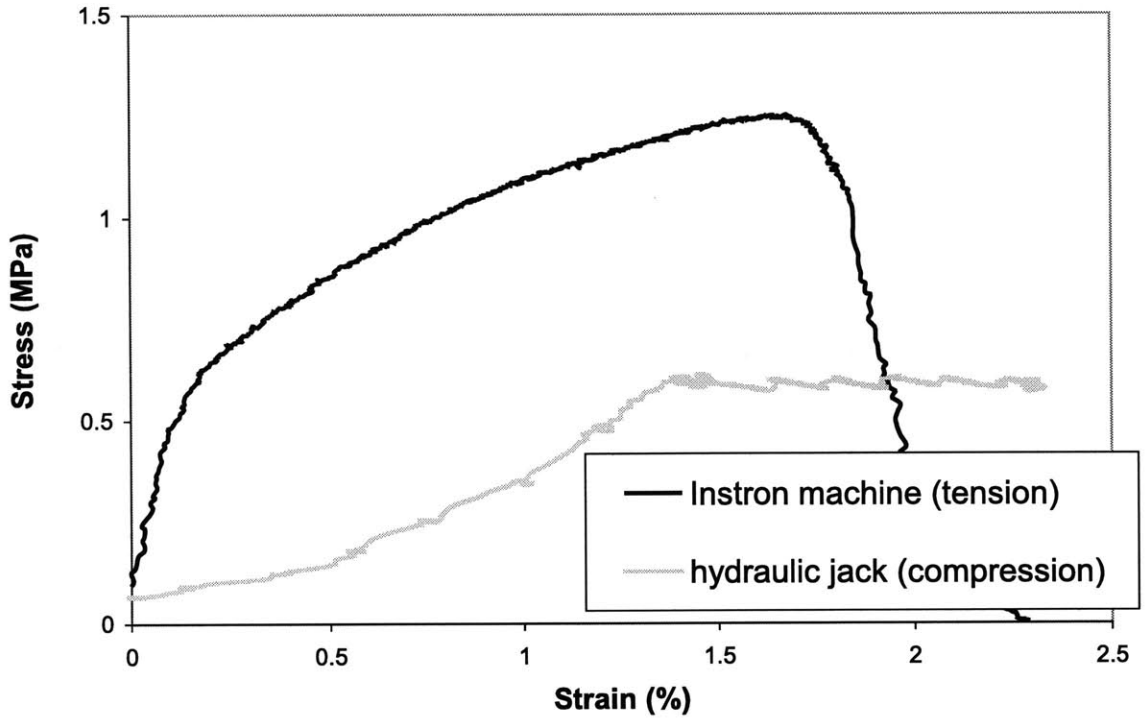

Figure 2.4: Typical biaxial stress-strain curves (compression-tension) for Alporas foam

points has been used (i.e. the directions have been inverted) to be more consistent with the other results. On the charts are also plotted the different criteria (Eqn 1.18, 1.22 and 1.24). The density of the foam was measured to compute GAZT criterion (average for Alporas: 0.216 g/cc, for ERG: 0.217 g/cc), and a value of the plastic Poisson's ratio measured by E. Andrews (Alporas: $\nu^p = 0.024$, ERG: $\nu^p = 0.052$) has been used to plot Miller's and Deshpande and Fleck's criteria.

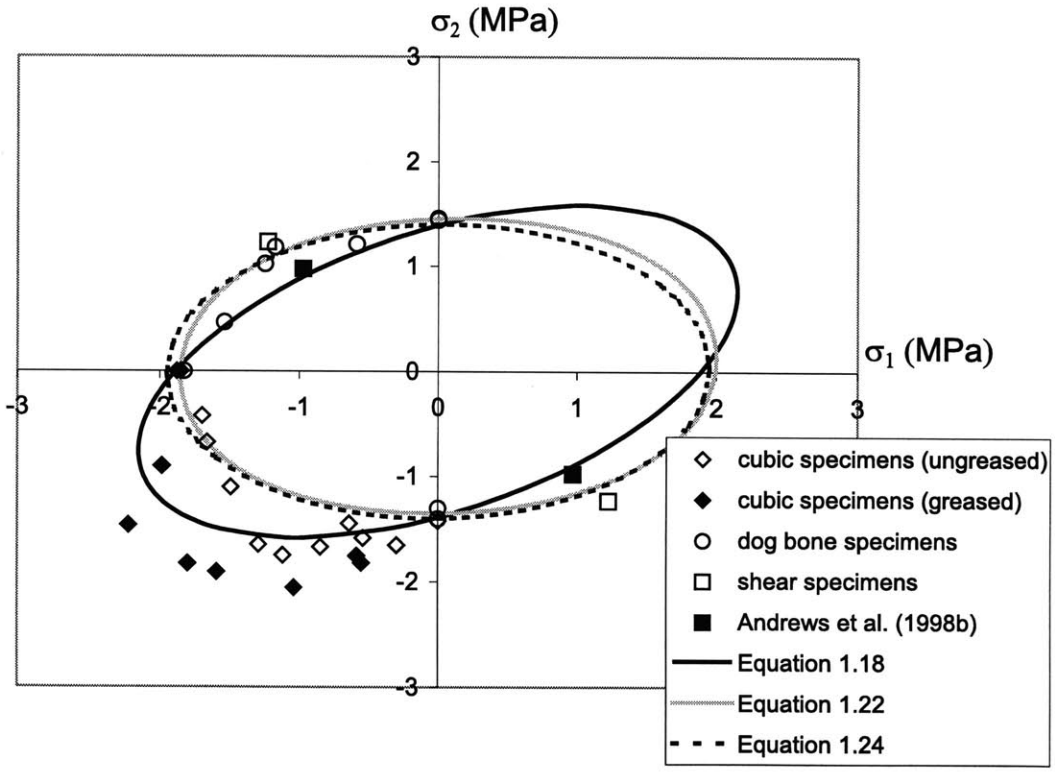

Figure 2.5: Biaxial results for Alporas

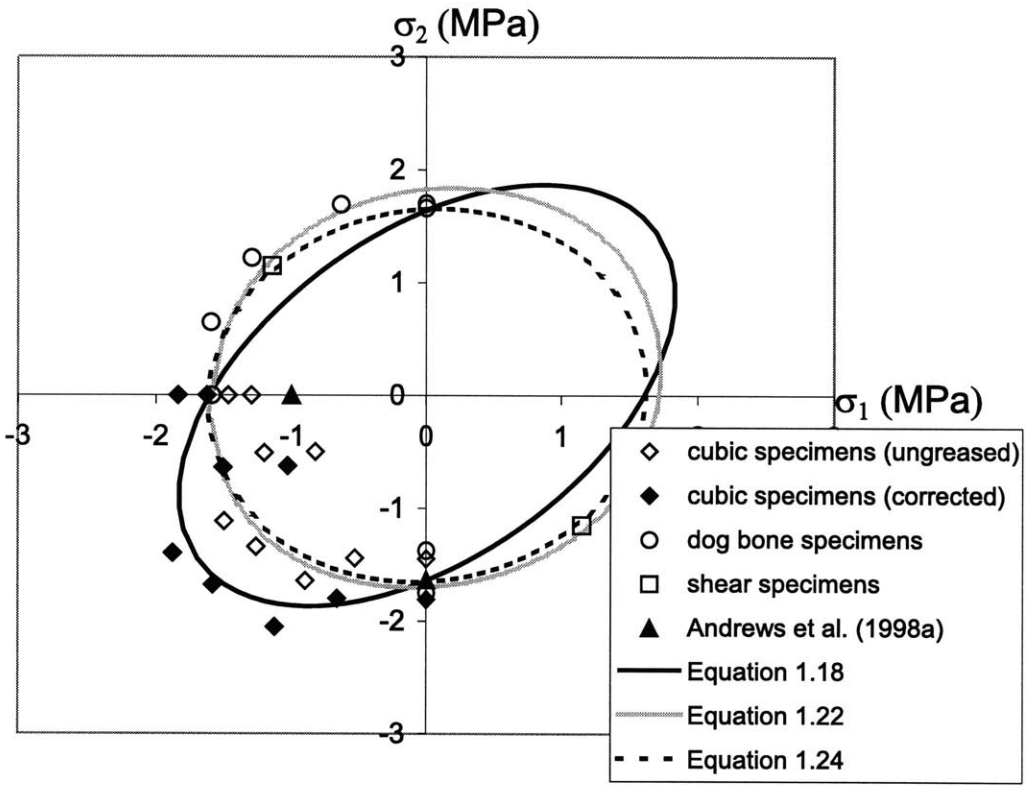

Figure 2.6: Biaxial results for ERG

2.5 Discussion

These results first show that Deshpande and Fleck's and Miller's criteria seem to describe the yield behavior of the foams better than GAZT criterion. Miller's criterion being more general than Fleck's one, it shows also the difference between the tensile and the compressive behavior. Triaxial tests done by McCormack (Gioux et al, 1998) show the same best fitting for Miller's and Fleck's criteria. From these experiments appears also the importance of friction in such setups. The struts or walls (depending on the kind of foam) have to be free to move perpendicularly to the plates or they generate some constraints in the structure. Some experiments in the tensile-tensile quadrant would help to validate the criteria, but this state of stress is difficult to obtain.

Chapter 3

Effect of cell size on the properties of aluminum foams

3.1 Objective

Models for the mechanical behavior of foams aim to describe them as a continuum. These continuum models are valid as long as a sufficient number of cells are involved: the properties are averaged over several cells and do not vary depending on the way the boundary cells are attached or damaged. But not included in these models is the special behavior of the foam structure when only a few cells are involved (for instance, in thin sandwich structures) : foam properties are then affected by the behavior of a few cells, and the way they are attached to the structure, or damaged is an important factor.

In this chapter, this "size effect" phenomenon is studied for several mechanical properties of foam structures. All the experiments described here have been done

on Alporas foam, which is described in Appendix A. Its resistance to axisymmetric indentation was studied first, with different sizes of indenters, then its shear strength was tested, using several thicknesses of foam. Another set of experiments was used to quantify the size effect on the shear modulus of the foam.

3.2 Indentation strength

3.2.1 Materials

All the indentation tests were performed on Alporas foam (cell size: 4.5 mm, see Appendix A for other characteristics). The blocks were cut using a band saw. The surface preparation technique (band saw, diamond saw,...) has little effect on the value of the mechanical properties of aluminum foams (eg Young's modulus, plastic collapse stress. Andrews et al., 1998). As a result, it was assumed that surface preparation would not be of crucial importance in the indentation tests.

Foam blocks were indented with cylindrical steel indenters with diameters of 6, 12, 24 and 30 mm and heights between 12 and 20 mm. Tests were performed with the indenter unbonded to the foam, allowing the walls of the foam to move under the indenter, and bonded to the foam to avoid any movement of the foam immediately beneath the indenter. In the experiments with indenters bonded to the foam, a

metal-based epoxy (J-B Weld, J-B Weld Company, Sulphur Springs, TX) was used. A thin film of epoxy was put on the indenters, and the blocks rested on the top of the indenters until the epoxy was solid, so that the epoxy did not infiltrate the cells and reinforce the walls and the cells under the indenter.

3.2.2 Method

The indenters were attached to the 10 kN load cell of an Model 1361 Instron (Canton, MA) testing machine. A block of Alporas aluminum foam was placed on the lower platen which was raised against the indenter at the speed of 0.05 mm/sec (Fig. 3.1). Displacements of the platen were known through the internal displacement measurement system of the testing machine. The resulting force and displacement were recorded through Labview data acquisition system (National Instruments, Austin, TX). Experiments were stopped when indenters had gone about 5 mm deep into the foam blocks (see photo on fig. 3.2). For each size of indenter and each configuration, at least three tests were performed.

In a first step, the influence of the thickness of the block of foam, and the influence of the distance of the indenters to the edges of the block were characterized. Such tests were necessary to be sure not to measure effects other than that due to the size of the indenter. The aim of these tests was to determine the thickness and distance

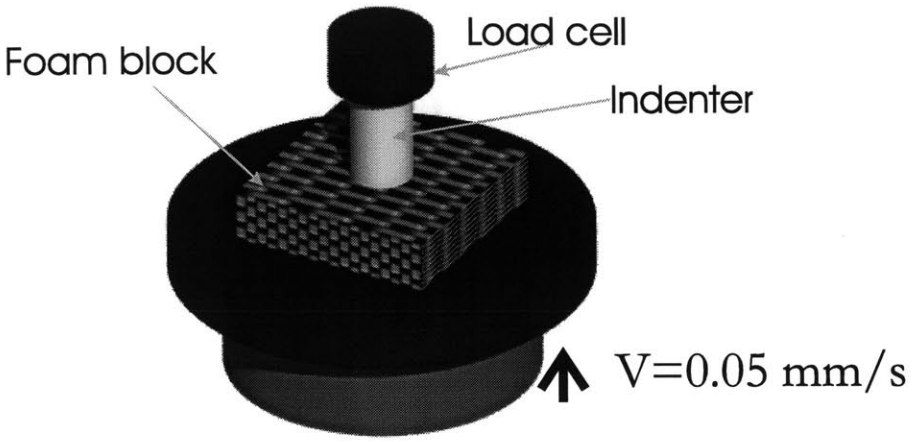

Figure 3.1: Setup of indentation tests

of the indenter from the edges above which the indentation strength is not influenced by these factors. Blocks with thicknesses equal to 1, 2 and 3 times the diameter of the cylinders were used. The results show that for any thickness greater than or equal to the diameter of the indenter, the curves obtained are roughly similar (Fig. 3.3). Similar experiments have been done with indenters distant from the edges by 1, 1.5 or 2 indenter diameters. The results (Fig. 3.4) show that a distance from the indenter to the edges of the block equal to the diameter of the indenter is sufficient to guarantee that the edges have no influence on the results. Therefore, in the tests for measuring the size effect in indentation, blocks of foam with thicknesses equal to 1.5 to 3 times the indenter diameter were used, and every indentation was distant from the edges and from other indentations by at least one indenter diameter. Those

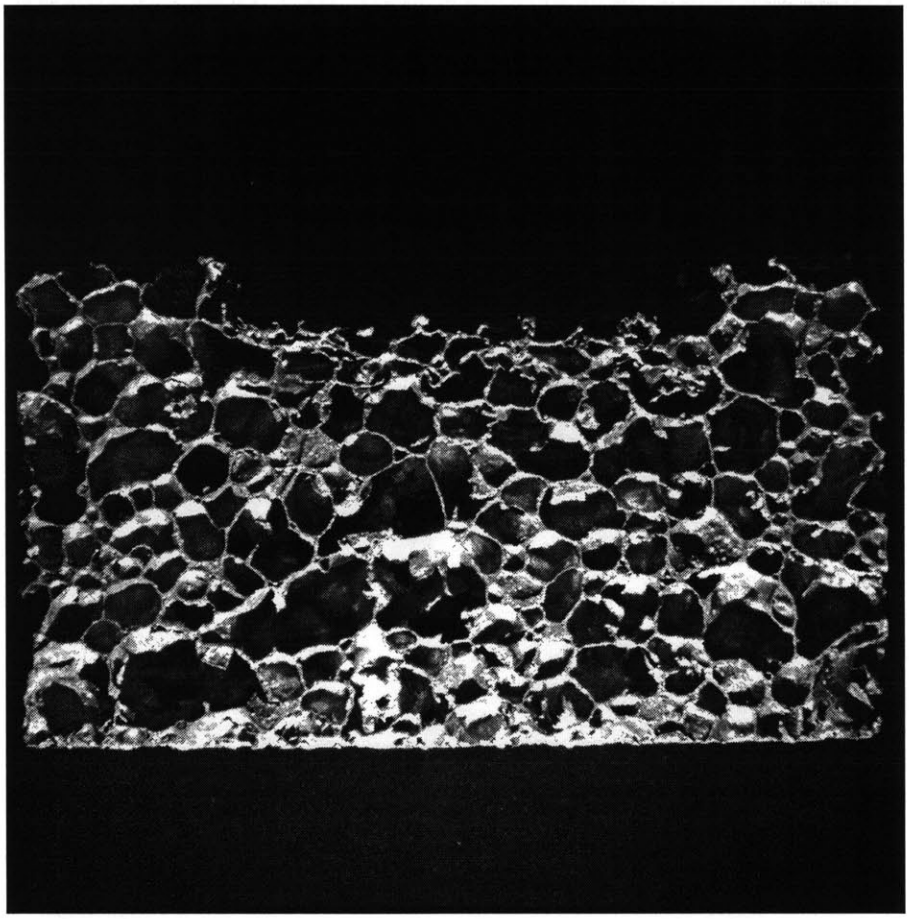

Figure 3.2: A block of foam after an indentation test

preliminary tests were performed with the biggest size of indenter (30 mm), so the tests with that indenter size were done with a thickness of 1.5 indenter diameter and a distance from the indenter to the edges or to the other tests of an indenter diameter. In the case of the smaller indenters, thicknesses greater than 1.5 indenter diameters and distances greater than one diameter were used: the smaller the indenters were, the greater the ratio between the thickness of the foam block or the distance from the indenter to the edges and the indenter diameter was chosen, to be sure not to introduce size effects other than the one studied in this part.

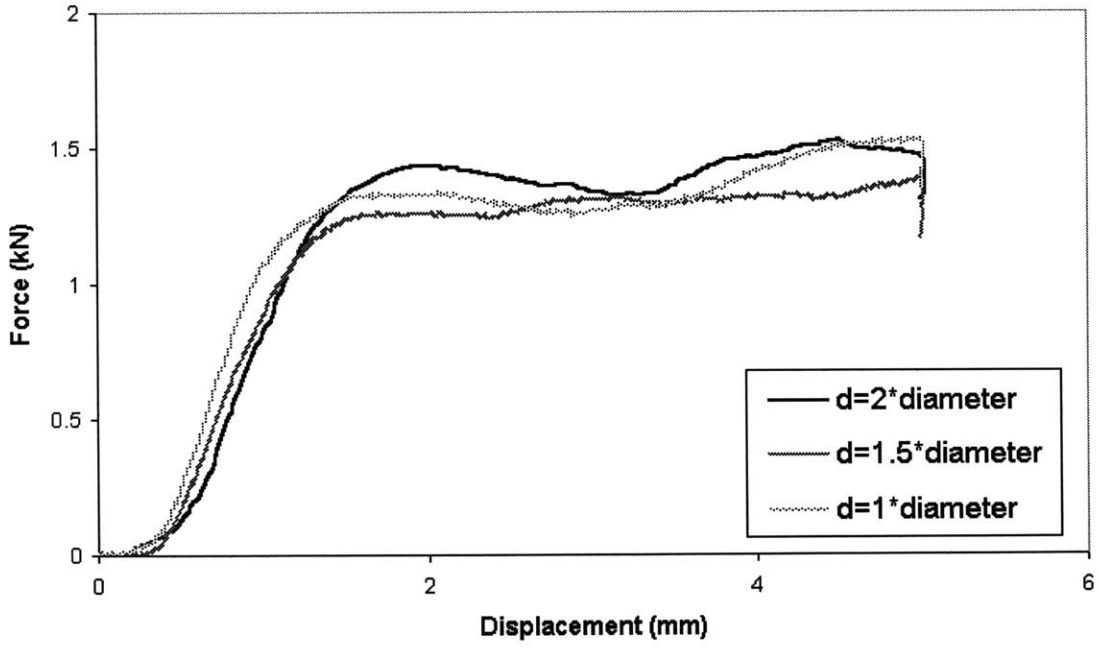

Figure 3.3: Influence of the thickness of the foam block (t) on the peak stress. Indenter diameter of 30 mm.

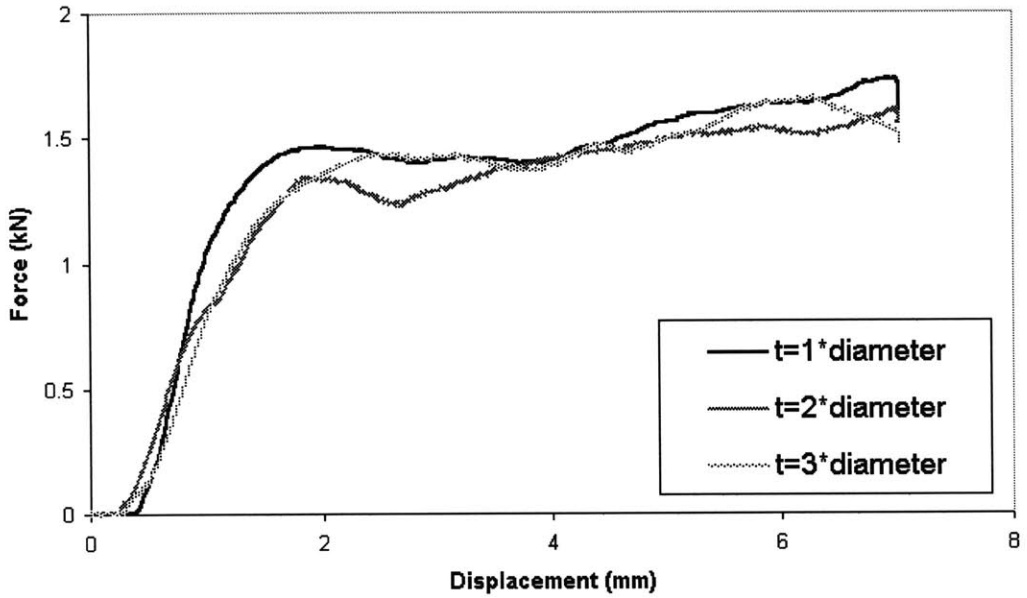

Figure 3.4: Influence of the distance from the edges (d) on the peak stress. Indenter diameter of 30 mm.

3.2.3 Results

Fig. 3.5 shows a typical stress-displacement curve obtained for a test with a non bonded indenter. Initially, the behavior of the foam is elastic, then it reaches a peak value $\sigma^{\star}_{ind}$ where the foam starts to yield plastically ($\sigma^{\star}_{ind}$ is either clearly defined, or determined at the intersection of the elastic slope and that of the yielding plateau). As the strain increases, the stress remains almost constant after that point. On Fig. 3.6, values of $\sigma^{\star}_{ind}$ are reported versus the diameter of the indenter used, for bonded

and non-bonded indenters.

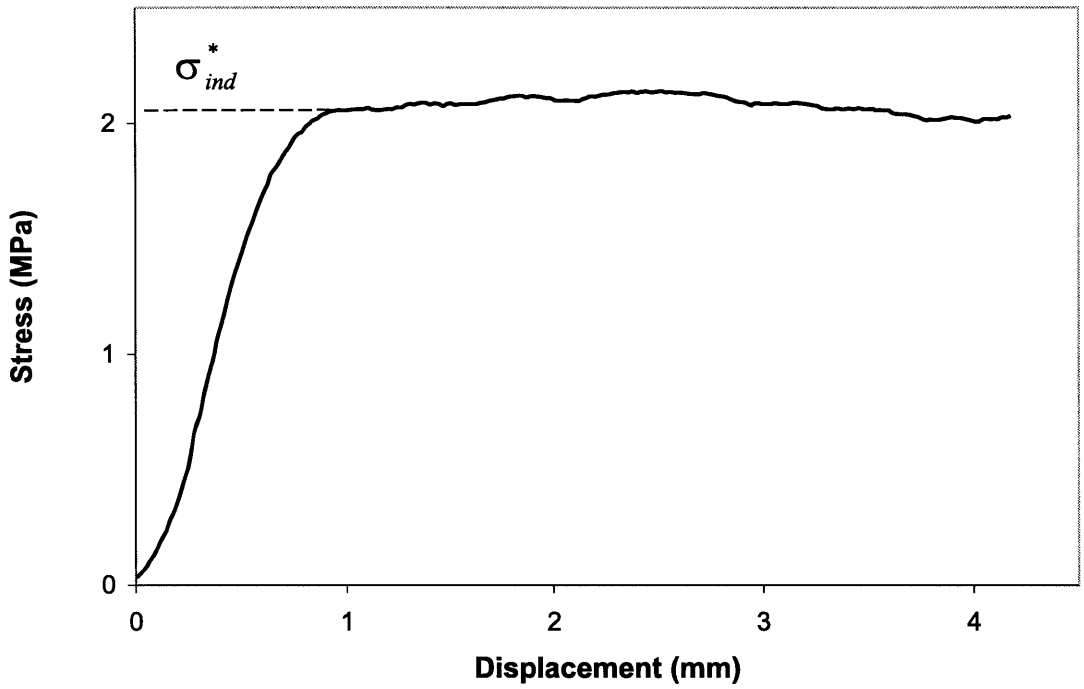

Figure 3.5: Typical stress-strain curve in indentation tests

This curve clearly shows the influence of the diameter of the indenter. For small sizes (less than 4 times the size of the cells), the peak stress tends to increase. For bigger indenter sizes, the peak stress reaches an asymptote, slightly above the uniaxial compressive strength of the foam (as expected since the plastic Poisson's ratio of the foam is almost equal to 0). Bonding indenters tends to increase the force necessary to indent the foam. But the shape of the curve stays the same, and the

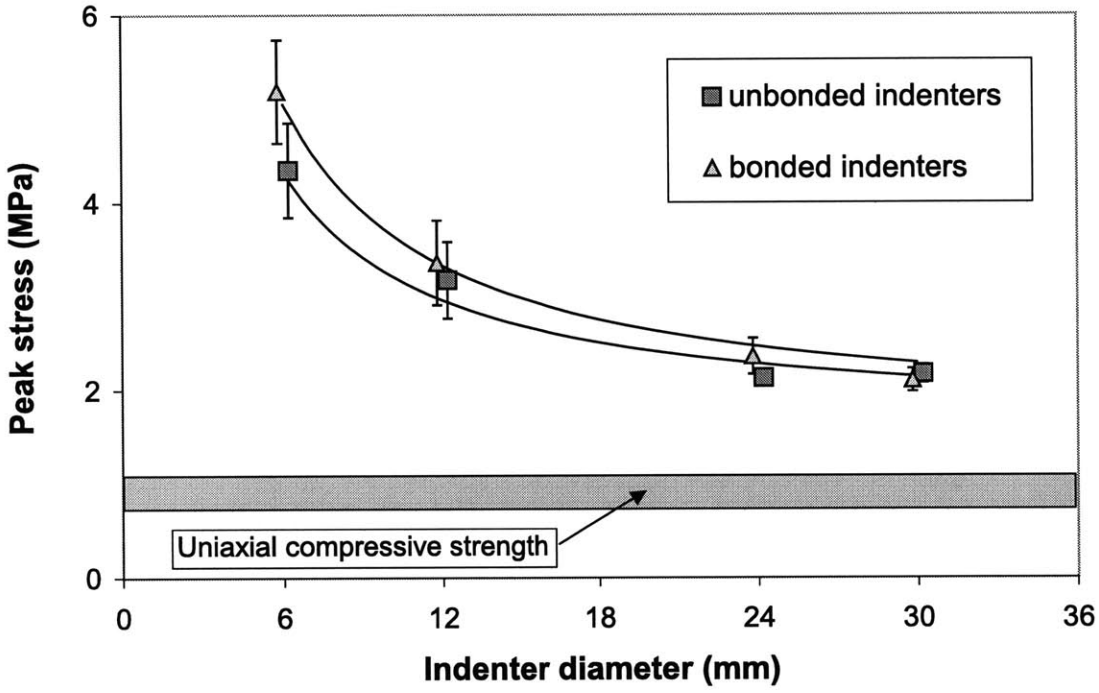

Figure 3.6: Results of indentation tests

stress has still to be higher to indent the foam with smaller indenter sizes.

3.2.4 Discussion

Two main conclusions come from the results described above. First, it can be noted that bonding the walls under the indenter makes the indentation strength higher ($\approx$ 10 % higher) for any size of indenter. When not bonded, the walls on the surface of the block can move and deform to accommodate the relative displacement of the indenter. When the walls are clamped, their deformation takes more energy and therefore increases the pressure necessary to crush them.

The second conclusion in these experiments is that, both in bonded and non-bonded experiments, we can note a size effect, which makes the indentation strength higher for small indenters. When using indenters with diameter higher than 18 mm (that is about 4 times the average size of Alporas cells), the size effect tends to disappear asymptotically and the indentation strength approaches the uniaxial compressive strength (as predicted by Wilsea et al., 1975). The diameter of the smaller indenter used in these experiments was about 1.3 times the average diameter of cells, and with such indenter, the indentation strength tends to increase by a factor of almost 2.

A possible explanation of this size effect is the following one: two different pro-

cesses occur when indentation occurs, the first one consisting of the crushing of the foam under the indenter, and the second one of yielding, then tearing the cell walls at the edge of the indenter (Fig. 3.7). The resulting indentation force is the sum of two forces:

$$\begin{aligned} F_{indentation} &= F_{crushing} + F_{tearing} \\ &= \sigma^{\star}_{pl}\pi r^2 + cd\tau^{\star}_{pl}2\pi r \end{aligned}$$

where r is the radius of the indenter, $\sigma^{\star}_{pl}$ the uniaxial compressive strength, $\tau^{\star}_{pl}$ the shear strength of the foam, and d the cell size. c is a constant. This gives, in term of stresses:

$$\sigma^{\star}_{ind} = \frac{P_{ind}}{\pi r^2} = \sigma^{\star}_{pl} + \frac{Cd\tau^{\star}_{pl}}{r} \tag{3.1}$$

Using $\sigma^{\star}_{pl} = 1.6$ MPa as found in uniaxial compressive tests (Andrews et al, 1998b), $\tau^{\star}_{pl} = 1.0$ MPa and $C = 3.63$, the agreement between this theory and the experimental results is satisfactory (Fig. 3.8).

This set of experiments exhibits another phenomenon specific to cellular structures that leads to a size effect. The size effect described here is not due to the damaged outer layer, nor to the elastic properties of the core. This type of size

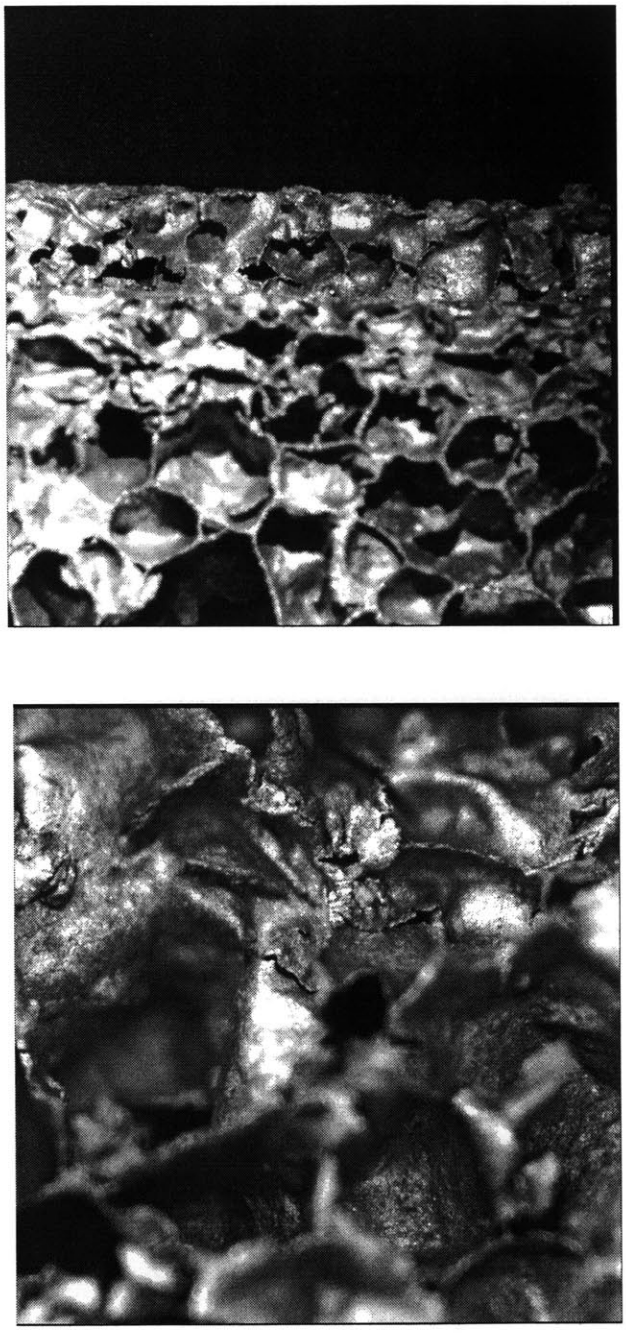

Figure 3.7: indentations tests: tearing of the cell walls

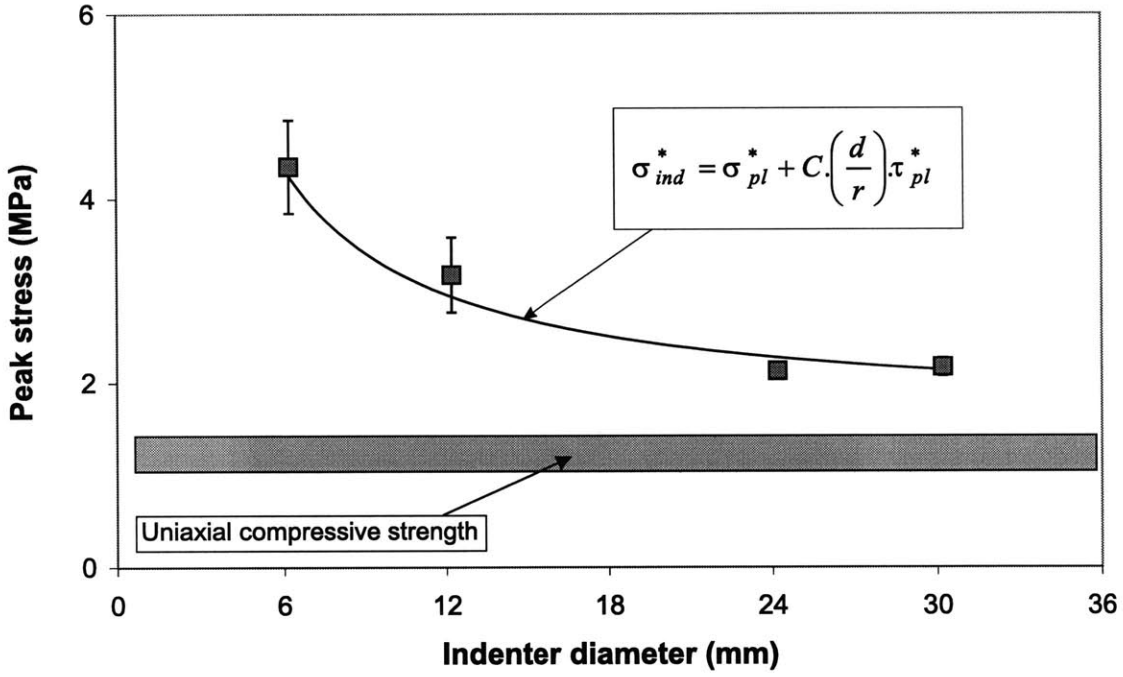

Figure 3.8: size effect in indentation tests: combination of 2 forces

effect is related both to the type of experiment and to the particular structure of foams. Sandwich structures failing in indentation of the core under certain conditions, this effect has to be taken into account to model the behavior of the structure.

3.3 Shear strength

3.3.1 Materials

The tests were performed on Alporas foam under shear stress according to the ASTM standard C273-94 "Standard Test Method for Shear Properties of Sandwich Core Materials" (Fig. 3.9). Five specimen sizes were tested, with thicknesses of 6, 12, 18, 24 and 30 mm. Their length was equal to 12 times the thickness and the width was constant (50 mm) (Table 3.1). These foam blocks were bonded to aluminum plates 12mm thick and 25 mm wider than the blocks. The Alporas foam blocks were cut using a band saw. The aluminum plates which the blocks were bonded to were prepared using a milling machine, so that their surface was rougher, and therefore improved the adhesion of the adhesive. The adhesive used to bond the foam blocks to the aluminum plates was the adhesive FM300, produced by Cytec (Havre de Grace, MD). The plates and the foam were cleaned with MEK (Methyl Ethyl Ketone), acetone, then alcohol, with drying periods between each step. The

specimens were then prepared, with a layer of adhesive between the plates and the foam block. They were placed into an autoclave and cured for one hour, at a pressure of 0.14 MPa and a temperature of 177°C. For the first batch of specimens, vacuum bagging was used to improve the contact between the components (pressure of 15 psi, with an added pressure of 25 psi applied by the autoclave). In the second batch, no vacuum bagging was used, and only the pressure by the autoclave was applied. The result was as good as for the first batch in the sense that both batches did not have any problem of debonding of the adhesive.

Table 3.1: Shear strength specimens dimensions

core thickness (mm)	length (mm)	width (mm)	number of specimens	average relative density
6	72	50	5	0.1889
12	144	50	6	0.2135
18	216	50	6	0.2122
24	288	50	6	0.2125
30	360	50	6	0.2086

3.3.2 Methods

The specimens were tested using an Model 1321 Instron testing machine (Canton, MA) in displacement control with a strain rate about 3.10^{-4} / sec. The force applied was measured using a 50 kN load cell and the displacements were measured using LVDTs (Model 0241, Transtek, Ellington, CT) mounted along the plates (Fig 3.9).

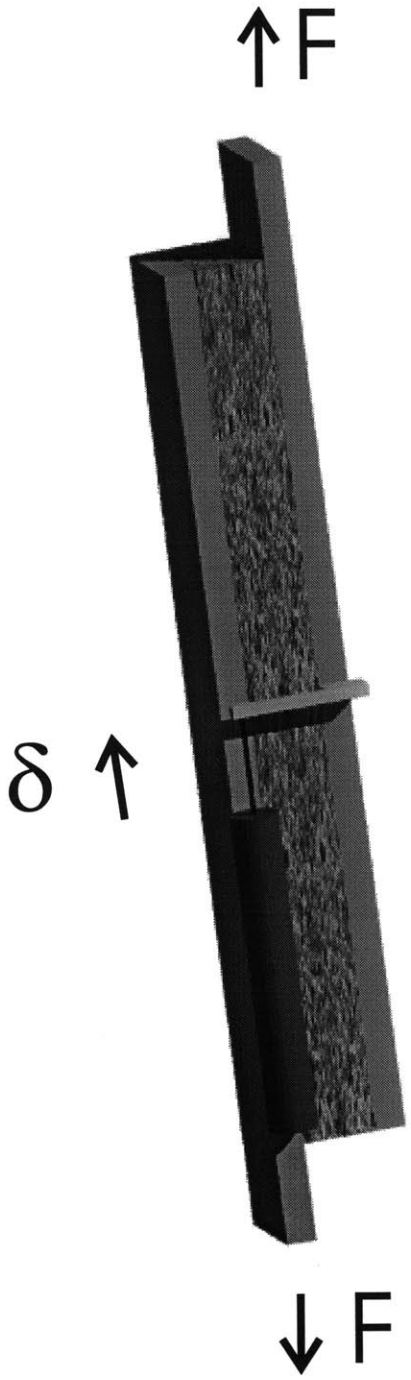

Figure 3.9: ASTM Standard for shear properties of sandwich core materials

All the results were obtained through Labview data acquisition system (National Instruments, Austin, TX).

3.3.3 Results

The ASTM standard gives a formula to compute the shear stress in the foam:

$$\tau = \frac{P}{L.b} \quad , \tag{3.2}$$

where τ is the core shear stress, P is the load on the specimen, L is the length of the specimen, and b is the width of the specimen. Fig. 3.10 shows a typical stress-strain curve obtained from this type of experiment. The stress reaches a peak, after which the material fails. After that point, as the strain increases, the stress gradually goes down to 0 and the specimens breaks in two parts, along the diagonal of the foam which is the axis of loading (Fig. 3.11).

Using equation 3.2, the peak stress for each specimen was computed, and the average for each size is reported on fig. 3.12. For specimens with thicknesses bigger than 12mm, two or three specimens per size were selected so that their average density was around 0.20 g/cc. The average of their strength was plotted. For the 6mm thick specimens, the densities had a higher dispersion (0.183, 0.1824, 0.1801, 0.189 and 0.2096 g/cc), and a lower average density than the rest of the specimens.

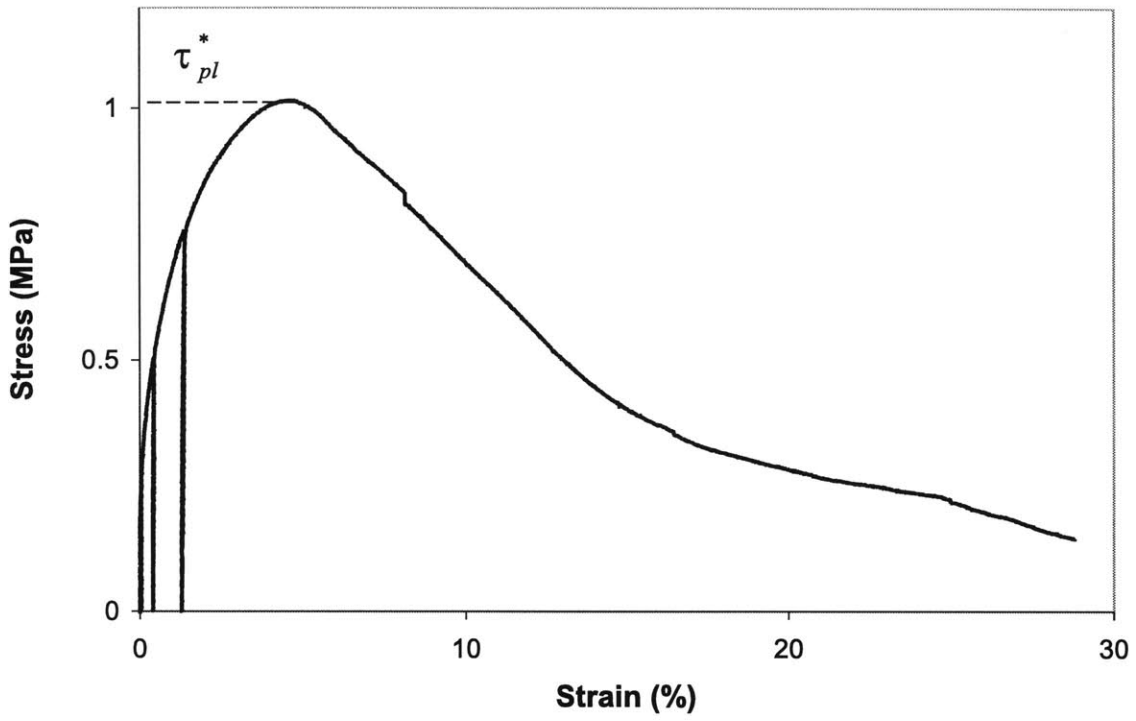

Figure 3.10: Typical stress-strain curve in shear experiments

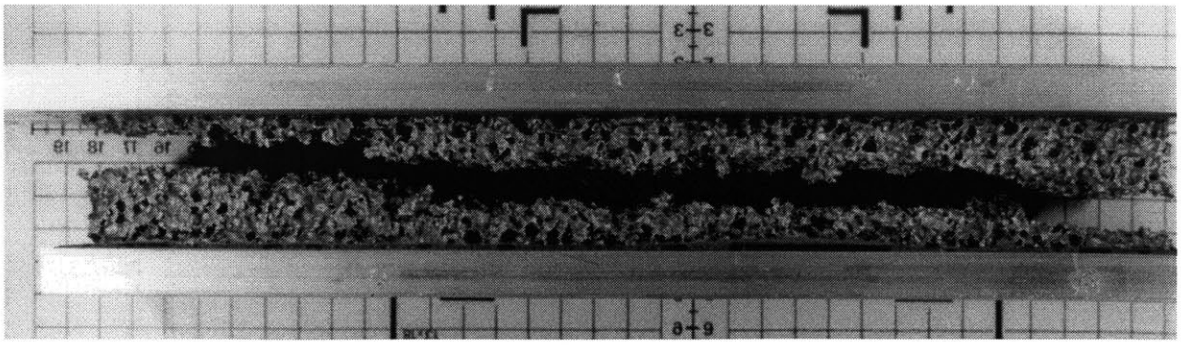

Figure 3.11: Photo of a shear specimen showing the failure plane along the diagonal of the specimen

Since the density has an influence on the shear strength, it was chosen to plot separately on Fig. 3.12 the specimens with the densities closest to 0.2 g/cc, that is the specimens with densities of 0.189 and 0.21 g/cc. Their average strength (1.5 MPa) was used to fit the line. All the results and densities can be found in Appendix B.

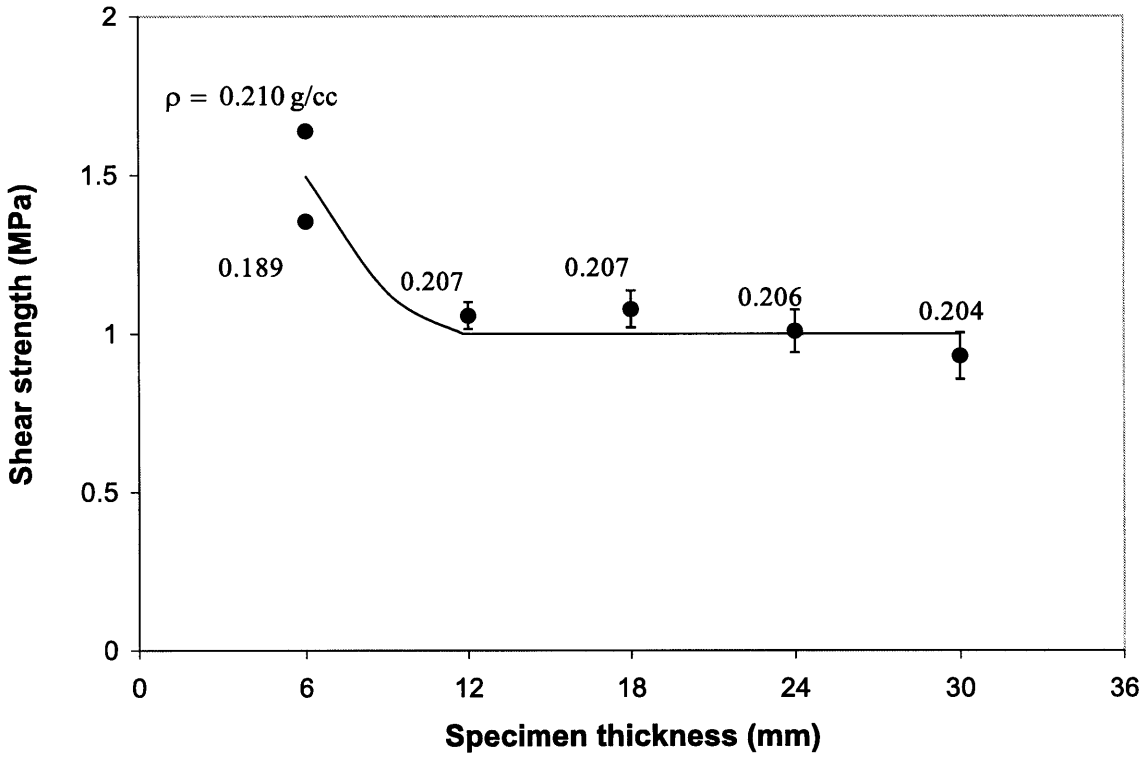

Figure 3.12: Size effect in shear strength experiments

The phenomenon of size effect can be noticed once again here. For thicknesses greater than about 3 cell sizes, the shear strength is almost constant. When the

thickness is smaller than that size, the shear strength increases.

Theoretically, it is possible to compute the shear modulus from this kind of experiment, unloading the specimens before the peak stress, and using the following formula:

$$G = \frac{S.t}{L.b} \quad ,$$

with G being the foam shear modulus, S the slope of the linear portion of load/ deflection curve during unloading, L and b respectively the length and width of the specimen. Two problems make this measurement difficult. First, the displacements in the unloading part of the curve are of the order of the micron (20 μm for the biggest specimens, 5 μm for the smallest), and measuring them requires very precise instrumentation. Second, finite element analysis indicated that bending of the attachment plates was significant (Fig. 3.13). Plate bending causes a rotation of the LVDT (depending on the place it is put on the plates), producing a relatively big error in the measurement of the displacement (very small itself). Using steel plates would not reduce the bending sufficiently. This ASTM standard was conceived for testing shear properties of honeycomb cores which are much more compliant than aluminum foams (Young's modulus for a typical aluminum honeycomb is 0.7 MPa, while it is around 1 GPa for Alporas foam). This method is not very well adapted to the measurement of the shear modulus of metallic foams.

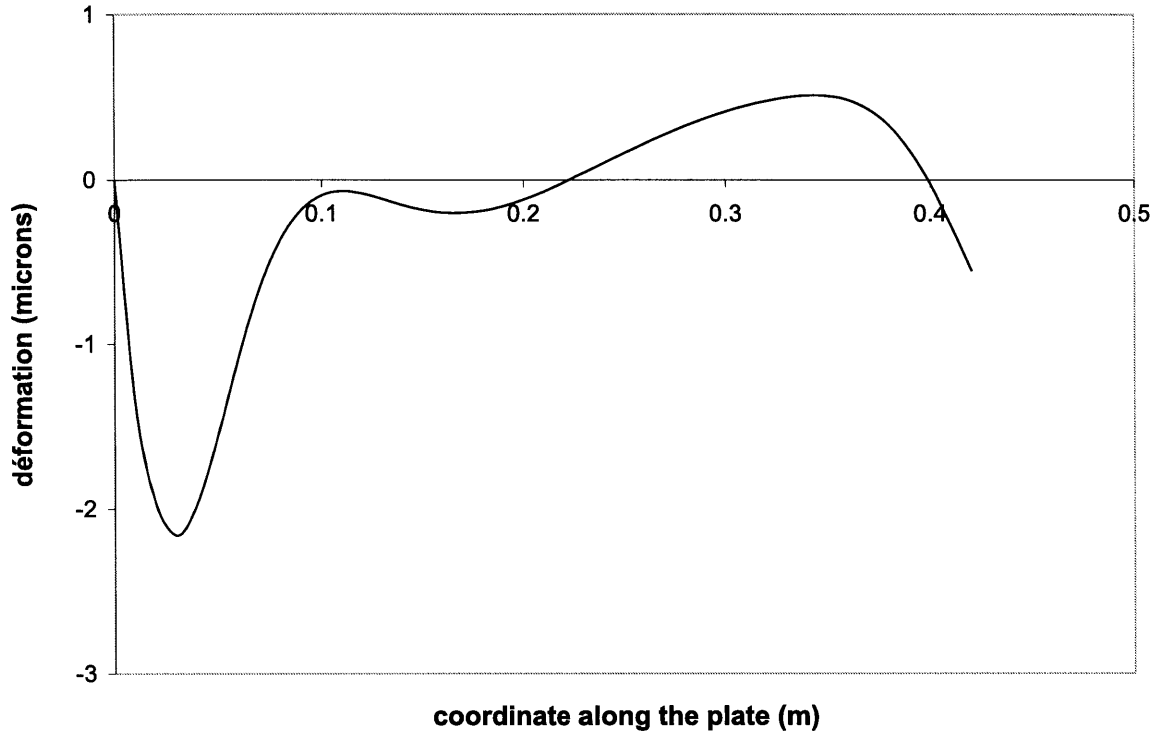

Figure 3.13: Bending of the plates (core thickness: 30 mm)

3.3.4 Discussion

This set of experiments shows that a size effect in shear strength can be expected for foams. This size effect disappears when considering specimens larger than about 3 cell sizes. This minimum number of cells is also the one that P. Onck (Andrews et al, 1998) found to characterize the disappearance of shear modulus size effect (analyzing a honeycomb structure with the same boundary conditions as in the experiments described above).

This increase in shear strength and modulus comes from the clamping of the cells on the boundaries. When using a thick core, many cells are free to deform, whereas in thin cores, almost all the cells are clamped, and it requires more energy to deform and break them. That explains this size effect in shear strength and modulus. The Brezny and Green's method could be applied to characterize this shear strength size effect, using an outer layer of cells with higher mechanical properties than the bulk: the adhesive holds the cell walls more rigidly than connected walls would have.

Many sandwich structures used typically can be considered as thin ones: the thickness of core used can be only two or three times the average cell size of the foam. This study shows that a strengthening effect can be expected from such thin cores : the shear strength of the core increases, increasing the strength of the whole structure.

Chapter 4

Stiffness and failure of sandwich beams

Using a failure criterion from chapter 2 (Miller criterion or Deshpande Fleck criterion), it is possible develop failure formula to be used when making the failure maps for sandwich beams with the Alporas or Duocel foam cores. Different aspects of size effects have been studied in chapter 3, allowing prediction of the influence of size effects on the stiffness and strength of sandwich beams when the thickness of the core is composed only of a few cells. This is the objective of this chapter.

4.1 Influence of shear modulus size effect on the stiffness of sandwich beams

As given by Allen (1969), the compliance of a sandwich beam is given by:

$$\frac{\delta}{P} = \frac{l^3}{B_1(EI)_{eq}} + \frac{l}{B_2(AG)_{eq}}. \tag{4.1}$$

B_1 and B_2 depend on the geometry of the loading (see table 4.1 for values).

Table 4.1: Constants for bending of beams

Mode of loading	B_1	B_2
Cantilever, end load P	3	1
Cantilever, uniformly distributed load $q = P/l$	8	2
Three-point bend, central load P	48	4
Three-point bend, uniformly distributed load $q = P/l$	384/5	8
Ends built in, central load P	192	4
Ends built in, uniformly distributed load $q = P/l$	384	8

$(EI)_{eq}$ and $(AG)_{eq}$ are defined by equation 1.25 and 1.26, which can be simplified (equations 1.27 and 1.28, adding the term $E_c bc/12$ in $(EI)_{eq}$, since it is no longer negligible) in the usual case where the faces are thin compared to the core. In that case, the compliance can be written:

$$K = \frac{\delta}{P} = \frac{2l^3}{B_1(E_f btc^2 + (E_c bc)/6)} + \frac{l}{B_2 bcG_c^\star}. \tag{4.2}$$

A size effect is introduced into the beam compliance through the shear modulus of the core. As described by Andrews et al. (1998), using either the Brezny and Green's analysis (1990), or using the simplified analysis of a honeycomb, the shear modulus of the core is expected to increase when the thickness of the core c decreases (because of the rigid clamping of the boundary cells).

If, as expected from the Brezny and Green's method (Eq. 1.35):

$$G_c^{\star} = \frac{G_{bulk}}{1 - A\frac{d_{cell}}{c}},$$

producing an increase of $G_c^{\star}$ when the thickness of the core is smaller than 3 or 4 cells, the part of the compliance due to shear can be written:

$$K_{shear} = \frac{l(1 - Ad_{cell}/c)}{B_2 bcG_{bulk}}.$$

The decrease of compliance due to the size effect can be measured by:

$$\tilde{K} - K = \tilde{K}_{shear} - K_{shear} = \frac{lAd_{cell}}{B_2 bc^2 G_{bulk}} \tag{4.3}$$

where $\tilde{K}$ is the compliance of the beam assuming there is no size effect. Eq. 4.3 shows that the size effects on shear modulus introduces a stiffening of sandwich beams with cores thinner than 3 or 4 cell diameters.

4.2 Failure equations for different modes of failure

For Alporas foam, as well as for Duocel foam, chapter 2 has shown that Miller's criterion allowed the best fit to the experimental data, and is the best to predict

when the foam fails. Based on this criterion, Miller (1998b) has derived equations describing the failure of sandwich structures with foam cores following his criterion, for different modes of failure. The three modes of failure found in experiments have been studied: yielding of the faces, indentation of the core, and shear failure of the core. The face wrinkling mode of failure described by Gibson and Ashby and not present in Miller's analysis is theoretically possible, but requires a very low relative density of the foam.

Defining $\tilde{P} = \frac{P}{bl\sigma_c}$, where P is the applied load, b the width of the sandwich, l its length and σ_c the uniaxial compressive strength of the core, Miller found the equations 1.30, 1.31 and 1.32 for the different modes, with the geometry described on Fig. 1.5. Using those equations, it is possible to build failure maps like the one shown on Fig. 4.1. The line on the map represents the points where both modes (shear failure and indentation) happen at the same load. Several parameters have to be defined before knowing what is the failure mode of a sandwich: the material of the face (E_f and σ_y), the foam (E_c, σ_c, parameters of the failure criterion), the different dimensions (t, c, l, r and b). Therefore, it is possible to plot failure maps using several parameters, assuming that the others are fixed.

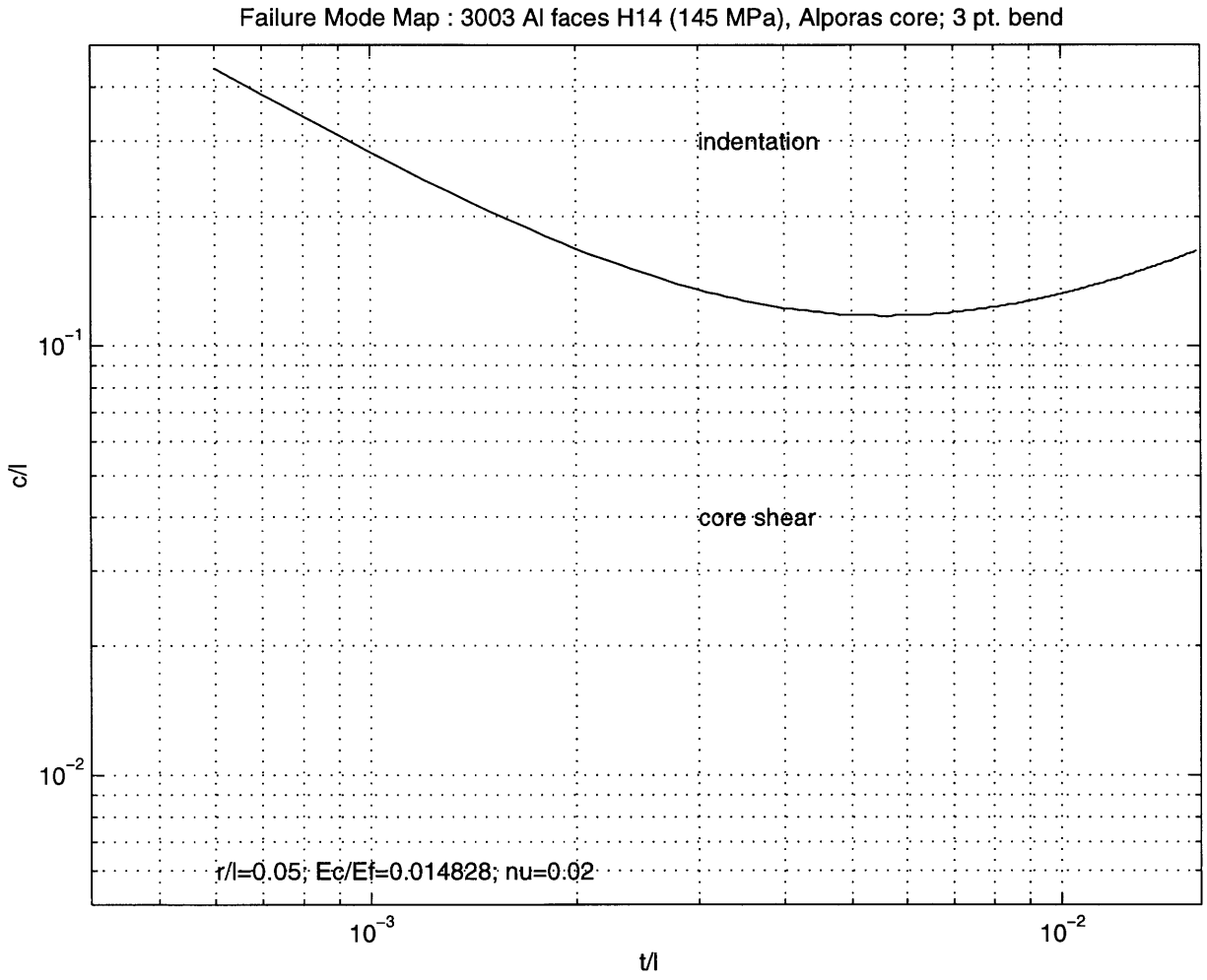

Figure 4.1: Failure map obtained from Miller's equations for failure

4.3 Influence of size effects on failure maps

The equations derived by Miller, and used to draw failure maps as described in the previous section, do not take into account the size effects described in chapter 3. The edge effects should appear in the failure criterion, since the stress required to fail by shear the core of a thin sandwich beam is higher than the bulk shear strength. A size effect specific to indentation has also been noticed for the foam. The influence of that size effect on sandwich beams failure has also to be studied.

- **Influence of edge effects**

  The increase in shear strength when the core thickness decreases makes it harder to fail the sandwich beam because of shear failure of the core. Therefore, shear strengthening edge effects are expected to move the frontier between face yielding and shear failure, and the frontier between indentation and shear failure, decreasing the size of the shear failure domain. For given beams dimensions, the strength of a sandwich beam with a thin core will be higher than expected from Miller's equations of failure, and it is possible that the beam fails in indentation or face yielding whereas the failure maps from Miller's equations showed shear failure of the core. Getting this strengthening effect incorporated in the failure maps would require modifying the failure criterion of the foam near the edges by increasing its strength. The failure equations would then

be modified taking into account the strengthening effect, and the failure map would show the reduction of the shear failure domain. Fig. 4.2 shows the evolution of the domains in a typical failure map when incorporating the size effect in the failure criterion. The shear strength of the sandwich beam is equal in this case to 1.5 times the shear strength of the bulk: incorporating in the criterion values of the unixial compressive and tensile strengths 1.5 times higher than that of the bulk, and assuming that the criterion is linear (Fig 2.5) in the compressive-tensile quadrant gives a shear stress 1.5 times higher than that of the bulk.

- **Influence of indentation size effect**

  The indentation size effect was observed with an indenter directly indenting the foam placed beneath it. The sandwich structure is different in the sense that a face sheet of metal is placed between the indenter and the foam. If the theory presented in chapter 3 is valid, the increase in indentation strength is due to the tearing of the cell walls around the indenter. When the pad is indenting the sandwich, it is not in direct contact with the foam. It deforms the face sheet, which indents the foam underneath. But there is no sharp edge indenting the foam nor tearing the cell walls. The indentation is progressive around the pad, the face sheet "spreading" the deformation over a large number of cells (Fig

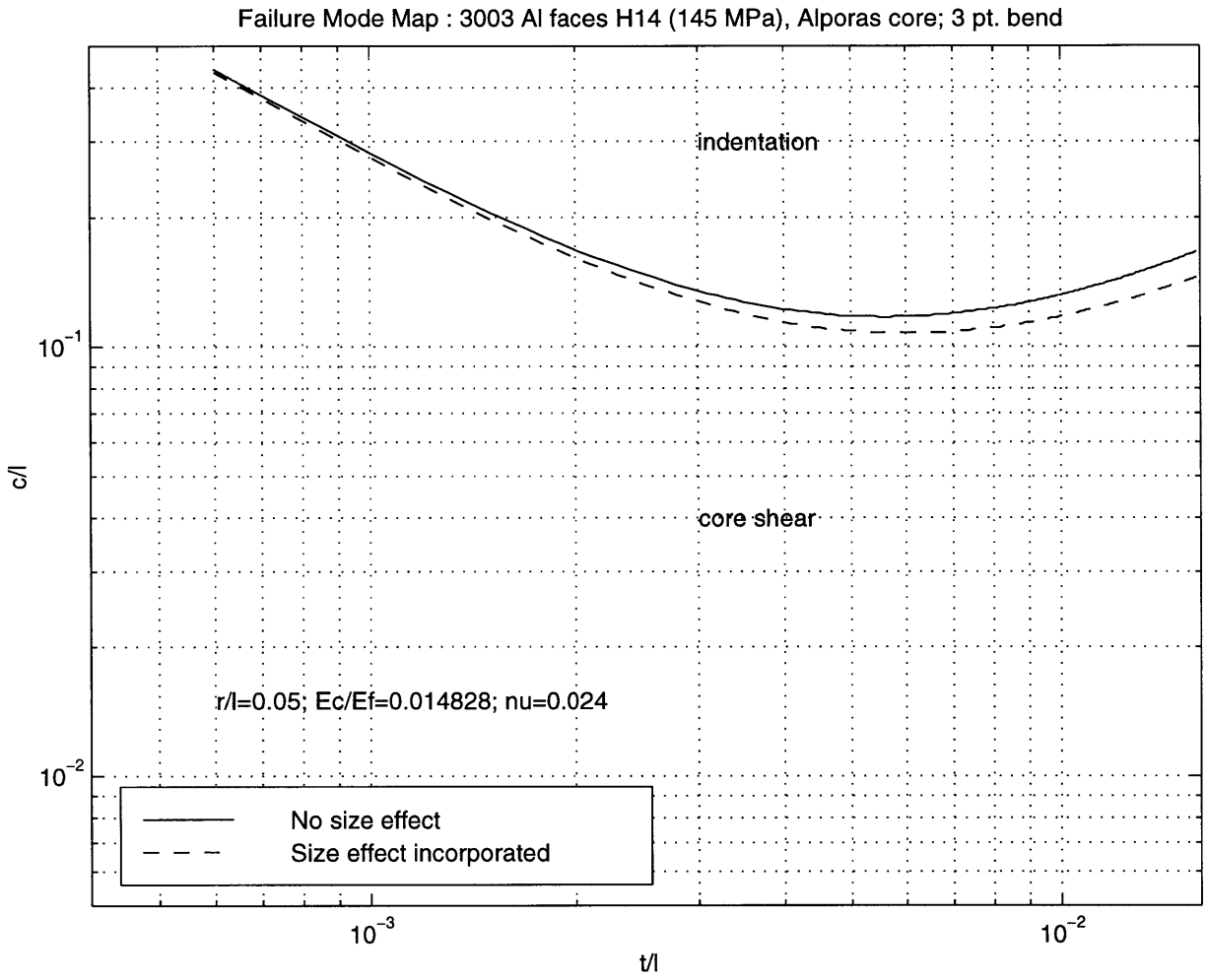

Figure 4.2: Failure map obtained from Miller's equations for failure

4.3).

Even in the case where the pads would be very small, the indentation size effect would not be observed in the indentation of sandwich beams. The only case where this size effect would appear is if a small pad broke the face sheet and then indented the foam underneath. But the failure would happen by the rupture of the face sheet, and before the indentation of the foam. Therefore, the indentation size effect has no influence on the strength of sandwich beams.

Of the two size effects that could have an influence on the failure of the sandwich beams, only the one due to edge effects (the clamping of the boundary cells increase the strength of the core) can be observed. This size effect has a strengthening effect on the sandwich, the load required to make it fail being higher than failure load given by equations not taking this effect into account (for instance Miller's equations). It can also affect the mode of failure of the beam: the failure maps built from the equations of failure not taking the size effect into account are modified by this strengthening effect and the domain of shear failure is smaller than expected from these equations.

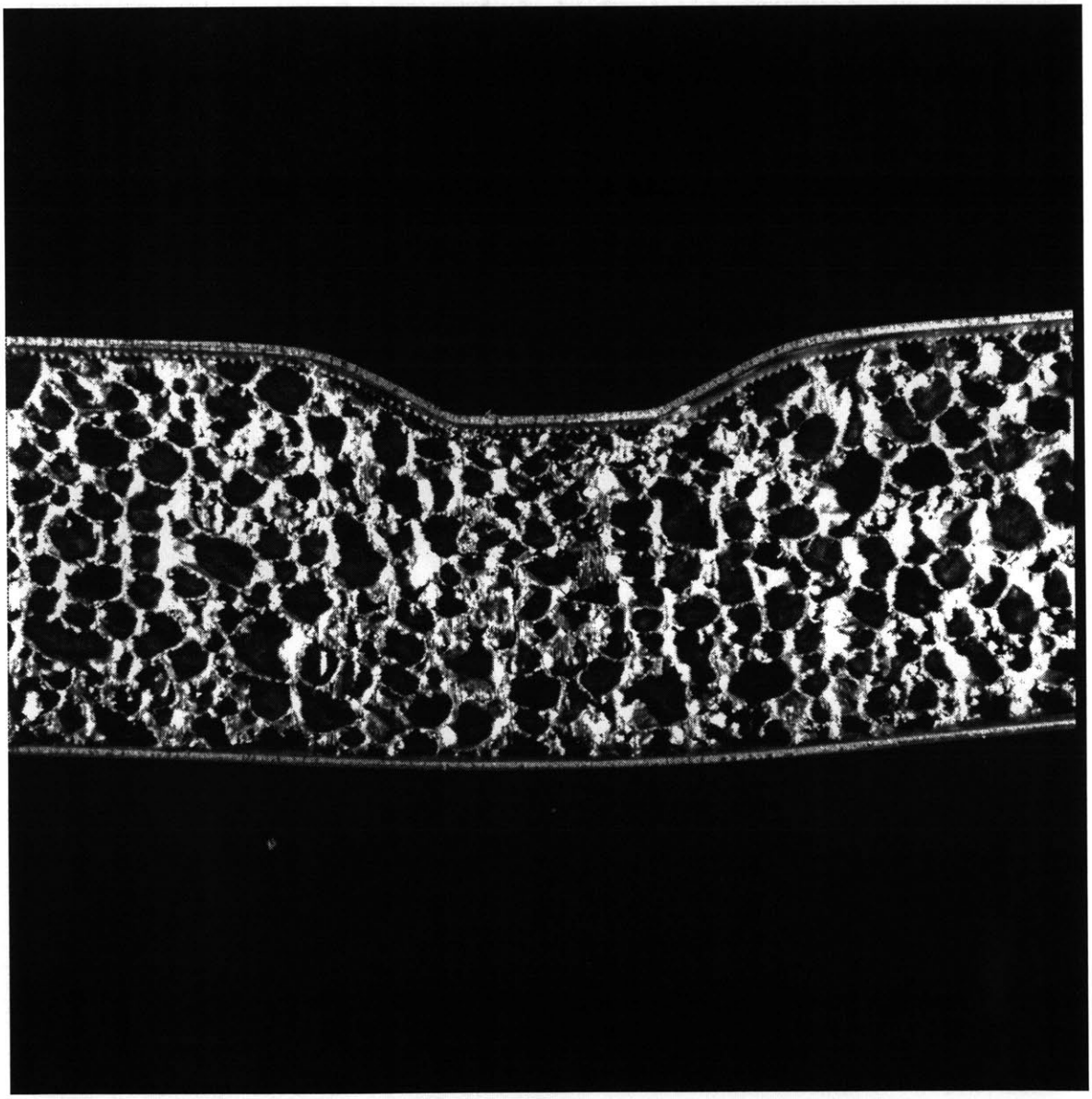

Figure 4.3: Indentation of a sandwich beam

Chapter 5

Conclusion

General equations are available to predict the behavior and failure of sandwich beams with foam core. They are based on the identification of a failure criterion for the foam, which gives the critical loads for different modes of failure. However, usually, sandwich structures have a thin foam core (a few cells across the thickness of the core). This introduces size effects in the behavior of the foam. The boundary cells are rigidly clamped to the plates, and since not many cells are in between the boundary cells, the properties of the core and of the sandwich are affected by the clamping: the sandwich is stiffer and stronger than expected from the equations using the bulk properties of the foam.

In this thesis, several failure criteria were compared over the biaxial failure of two foams, and two of them describes adequately the failure of foam structures. Different

size effects were studied: the influence of specimen thickness on shear strength, and the size effect on indentation strength. Using those last results and the models for influence of size on shear modulus, the influence of sandwich thickness on its stiffness and strength was studied. It was qualitatively appreciated how the predictions based on equations that do not take size effects into account would evolve if such effects were taken into account, to more accurately describe the behavior and failure of sandwich beams.

Further study of this subject could consist of several steps. The influence of core thickness on shear modulus already studied theoretically could be verified experimentally to obtain a precise relation between the core thickness and shear modulus, that could be used to compute exactly the stiffness of a sandwich beam, taking the size effects into account. Incorporating the size effect into the failure criterion of the foam would also help to get precise knowledge of the failure load of a sandwich beam when thin core is used, as well as a precise prediction of its failure mode.

Appendix A

Materials

A.1 Alporas

Supplier	Shinko Wire Company Ltd
address	10-1, Nakahama-machi, Amagasaki-shi 660 Japan
tel	+0081 6 411 1081
fax	+0081 6 411 1056
General Properties	mean (std dev)
Anisotropy ratio (a/b)[1]	1.0298 (0.0136)
Cell size	4.5 mm (4.65)
Density	0.21598 g/cc (0.00888)
Mechanical Properties	mean (std dev)
Compressive strength (direction 1)[2]	1.366 MPa (0.108)
Compressive strength (direction 2)[2]	1.600 MPa (0.067)
Densification strain[3]	63.671 % (0.585)
Young's modulus (direction 1)[2]	1.209 MPa (0.095)
Young's modulus (direction 2)[2]	0.867 MPa (0.078)
Shear modulus	246.25 MPa (28.211)
Shear strength	1.025 MPa (0.009)

[1] a and b are the maximum and minimum ellipse dimensions
[2] Tests by A. Simone
[3] Tests by E. Shepherdson

A.2 Duocel

Supplier	Energy Research and Generation, Inc
address	900, Stanford Avenue
	Oakland, CA 94608 USA
tel	+001 510 658 9785
fax	+001 510 658 7428
General Properties	mean (std dev)
Anisotropy ratio (a/b)[1]	1.1 - 1.3
Cell size	1.45mm - 1.6mm
Density	0.2171 g/cc (0.0061)
Mechanical Properties[2]	mean (std dev)
Compressive strength (loading direction parallel to cell elongation)	1.635 MPa (0.161)
Compressive strength (loading direction perpendicular to cell elongation)	0.996 MPa (0.12)
Densification strain (parallel)	69.5 % (7.78)
Densification strain (perpendicular)	63 % (3.46)
Young's modulus (parallel)	0.473 MPa (0.044)
Young's modulus (perpendicular)	0.206 MPa (0.024)
Shear modulus (parallel)	0.071 GPa (0.008)
Shear modulus (perpendicular)	0.0496 GPa (0.003)
Shear strength (parallel)	1.1866 MPa (0.1986)
Shear strength (perpendicular)	1.123 MPa (0.0586)
Tensile strength (parallel)	1.933 MPa (0.293)
Tensile strength (perpendicular)	1.078 MPa (0.17456)

[1] a and b are the maximum and minimum ellipse dimensions

[2] Tests by E. Andrews

Appendix B

Results tables

B.1 Biaxial results

Alporas[1]			**Duocel**[1]		
Specimen	σ_1(MPa)	σ_2(MPa)	Specimen	σ_1(MPa)	σ_2(MPa)
Cubic Specimens[2]					
31	-1.038	-2.057	2	-1.131	-2.052
32	-1.852	0	3	-1.035	-0.626
34	-1.597	-1.908	4	-1.878	-1.395
36	-0.553	-1.821	6	0	-1.808
37	-1.983	-0.903	7	-1.626	0
38	-2.219	-1.464	8	-0.667	-1.8
39	-0.585	-1.755	11	-1.84	0
40	-1.879	0	14	-1.585	-1.68
41	-1.802	-1.829	15	-1.509	-0.641
Dogbone specimens					
1	0	1.457	1	0	1.6625
2	0	1.4415	2	0	1.702
3	0	-1.302	3	0	-1.75
4	0	-1.402	4	0	-1.375
5	-1.25	1.02	6	-1.3	1.22

[1] σ_1: horizontal laod applied with the jig, σ_2: vertical load applied via the testing machine

[2] Corrected values for Duocel specimens, see chapter 2 for explanation

Specimen	σ_1(MPa)	σ_2(MPa)	Specimen	σ_1(MPa)	σ_2(MPa)
Dogbone specimens					
6	-1.177	1.181	7	-0.639	1.692
7	-1.83	0	8	-1.6	0.65
9	-0.587	1.21	9	-1.593	0
12	-1.544	0.465			
Shear specimens					
	0.9743	-0.9743		1.15	-1.15
	-0.9743	0.9743		-1.15	1.15

B.2 Indentation tests

Specimen	$\sigma^{\star}_{ind}$ **(MPa)**	**Specimen**	$\sigma^{\star}_{ind}$ **(MPa)**
Unbonded indenters		*Bonded indenters*	
6mm indenter diameter			
u6-1	4.92	b6-1	5.73
u6-2	3.89	b6-2	4.63
u6-3	3.71	b6-3	5.2
u6-4	4.42		
u6-5	4.91		
u6-6	4.24		
average	4.35		5.18
std dev	0.5		0.55
12mm indenter diameter			
u12-1	3.54	b12-1	4.03
u12-2	3.61	b12-2	3.05
u12-3	3.02	b12-3	3.21
u12-4	2.61	b12-4	3.14
u12-5	3.10		
average	3.176		3.36
std dev	0.41		0.45
24mm indenter diameter			
u24-1	2.056	b24-1	2.332
u24-2	2.122	b24-2	2.122
u24-3	2.133	b24-3	2.586
u24-4	2.21	b24-4	2.396
average	2.13		2.36
std dev	0.06		0.19
30mm indenter diameter			
u30-1	2.085	b30-1	2.221
u30-2	2.099	b30-2	1.982
u30-3	2.235	b30-3	2.019
u30-4	2.278	b30-4	2.201
average	2.174		2.106
std dev	0.096		0.123

B.3 Shear strength

Specimen	shear strength (MPa)	Density
thickness = 6 mm		
5.4[1]	1.638	0.2096
5.5[1]	1.355	0.189
5.7	1.06	0.182
5.8	1.109	0.18
5.9	1.156	0.183
thickness = 12 mm		
4.4	1.146	0.215
4.5[1]	1.027	0.204
4.6[1]	1.088	0.2105
4.7	1.26	0.2231
4.8	1.258	0.2155
4.9	1.242	0.213
thickness = 18 mm		
3.4[1]	1.01	0.2004
3.5	1.12	0.2181
3.6[1]	1.111	0.2096
3.7[1]	1.114	0.2094
3.8	1.1972	0.2257
3.9	1.108	0.2098
thickness = 24 mm		
2.4[1]	1.08	0.2149
2.5	1.07	0.2265
2.6	1.02	0.2167
2.7	0.932	0.2149
2.8[1]	1.00	0.202
2.9[1]	0.945	0.1997
thickness = 30 mm		
1.4	0.9449	0.2182
1.5	0.994	0.209
1.6[1]	0.984	0.2061
1.7	1.013	0.2125
1.8[1]	0.959	0.2053
1.9[1]	0.8456	0.2002

[1]Used on Fig. 3.12. See chapter 3 for explanation

Bibliography

[1] H.G. Allen. *Analysis and Design of Structural Sandwich Panels.* Pergamon Press, 1969.

[2] W.B. Anderson, C.P. Chen, and R.S. Lakes. Experimental study of size effects and surface damage in closed-cell polymethacrylimide and open-cell copper foam. *Cellular Polymers*, 13:1–15, 1994.

[3] E. Andrews, G. Gioux, and L.J. Gibson. The role of specimen size, specimen shape and surface preparation in mechanical testing of aluminum foams. To be submitted, 1998.

[4] E. Andrews, W. Sanders, and L.J. Gibson. Compressive and tensile behaviour of aluminum foams. To be submitted, 1998b.

[5] M.F. Ashby, A.G. Evans, J.W. Hutchninson, and N.A. Fleck. *Metal Foams: a Design Guide*, 4th edition, August 1998.

[6] R. Brezny and D.J. Green. Characterizattion of edge effects in cellular materials. *J. Materials Science*, 25:4571–4578, 1990.

[7] V. Deshpande and N.A. Fleck. A phenomenological constitutive model for metallic foams. To be submitted, 1998.

[8] D.C. Drucker and W. Prager. Soil mechanics and plastic analysis or limit design. *Q. Appl. Math.*, 10:157–165, 1952.

[9] N.A. Fleck, L.T. Kuhn, and R.M. McMeeking. Yielding of metal powder bonded by isolated contacts. *J. Mech. Phys. Solids*, 40:1139–1162, 1992.

[10] M.A. Fortes, J.J. Fernandes, I. Serralheiro, and M.E. Rosa. Experimental determination of hydrostatic compression versus volume change for cellular solids. *J. Testing and Evaluation*, 17:67–71, 1989.

[11] L.J. Gibson and M.F. Ashby. *Cellular Solids: Structure and Properties.* Cambridge University Press, 2nd edition, 1997.

[12] G. Gioux, T.M. McCormack, and L.J. Gibson. Failure of aluminum foams under multiaxial loads. To be submitted, 1998.

[13] T.M. McCormack. Master's thesis. To be published, 1999.

[14] R.E. Miller. private communication, 1998b.

[15] R.E. Miller and J.W. Hutchinson. A continuum plasticity model for the constitutive behaviour of foamed metals. To be submitted to Int. J. Mech. Sci., 1998.

[16] M.R. Patel. *The deformation and fracture of rigid cellular plastics under mutiaxial stress.* PhD thesis, University of California, Berkeley, 1969.

[17] M.C. Shaw and T. Sata. The plastic behavior of cellular materials. *Int. J. Mech. Sci.*, 8:469, 1966.

[18] T.C. Triantafillou. *Multiaxial failure criteria for cellular solids.* PhD thesis, Massachusetts Institute of Technology, 1989.

[19] T.C. Triantafillou and L.J. Gibson. Multiaxial failure criteria for brittle foams. *Int. J. Mech. Sci.*, 32:479–496, 1990.

[20] T.C. Triantafillou, J. Zhang, J. Shercliff, L.J. Gibson, and M.F. Ashby. Failure surfaces for cellular materials under multiaxial loads - ii: Comparison of models with experiment. *Int. J. Mech. Sci.*, 31:665–678, 1989.

[21] M. Wilsea, K.L. Johnston, and M.F. Ashby. Indentation of foamed plastics. *Int. J. Mech. Sci.*, 17:457–460, 1975.